

DELFT UNIVERSITY OF TECHNOLOGY

DEPARTMENT OF ELECTRICAL ENGINEERING, MATHEMATICS AND COMPUTER
SCIENCE

B.SC. GRADUATION THESIS

Current Sensor with CAN Interface and Capacitive Tire Wear Sensor

Authors:

Meriç Erceylan, 4305558
Koen Goedemondt, 4291077

July 15, 2018

This thesis was written in accordance with:

Dr. Ir. Chris Verhoeven	Supervisor
Dr. Ir. Ioan Lager	BAP supervisor B.Sc. Electrical Engineering
Casper van Wezel, BSc	Nuon Solar Team

Special thanks to:

Dr. Ir. Bart Roodenburg	Testing and measurement equipment
Dr. Fabio Sebastiano	Consulting

Abstract

This thesis covers the research, design process and testing of a new current sensor for the Nuon Solar Team. Hall effect and magnetoresistive based current sensors are investigated and compared to a shunt resistor based current sensor. It will become clear that for the needs of the Nuon Solar Team, a shunt resistor based current sensor is the best choice. Additionally, a capacitive tire wear sensor is covered. The wear is defined as thickness of the rubber, which will be sensed by the change in relative permittivity between capacitor plates. Thus resulting in a change in capacitance, which is measured using a charge amplifier circuit. The charge amplifier yielded a measurable voltage difference between a new and worn tire for static conditions. For dynamic conditions the motor PWM signal caused excessive amounts of noise, hence filtering is required at the discussed frequencies. Further recommendations are given for successful implementation of the capacitive tire wear sensor.

Contents

Preface	1
I Current sensor	2
1 Introduction	4
1.1 Problem definition	4
1.2 Scope	4
2 Requirements	5
3 Theoretical background	6
3.1 Hall effect	6
3.1.1 Open loop Hall sensors	6
3.1.2 Closed loop Hall sensors	6
3.2 Magnetoresistance	7
3.3 Galvanic isolation	7
4 Design	8
4.1 Coulomb counting	8
4.2 Temperature	11
4.3 Sensor comparison	11
4.4 LTSR 15-NP	12
4.4.1 Internal circuit	12
5 Testing	13
6 Results	16
6.1 Linearity	17
6.2 Temperature offset	17
6.3 Noise sources	17
6.3.1 Electromagnetic interference	17
6.3.2 Unpredictable offset problems	17
6.3.3 Questionable robustness	18
6.4 Comparison to shunt	18
6.4.1 Power consumption	19
7 Conclusion	21
7.1 Further work	21

II	Tire wear sensor	22
1	Introduction	24
2	Requirements	25
3	Theoretical background	26
3.1	Capacitance	26
3.2	Wheel capacitance model	26
3.3	Measuring capacitance	29
3.3.1	Current measurement through capacitor	29
3.3.2	Measuring permittivity difference of rubber for different frequencies	29
3.3.3	Frequency measurement of oscillator	29
3.4	Permittivity	30
3.4.1	Rubber	30
3.4.2	Air	30
4	Design	32
4.1	Measuring current through a capacitor	32
4.2	Frequency	35
4.2.1	Mechanical noise	35
4.2.2	Permittivity	36
4.2.3	Gain Bandwidth Product	36
4.3	Decoding the signal	37
4.3.1	AC to DC conversion	37
4.3.2	DC processing	38
4.4	Operational amplifier	39
4.5	Supply voltage and alternating signal	39
5	Simulations	42
5.1	Ngspice	42
5.2	KiCad	42
5.3	Python parser	42
5.4	Gain phase simulations	43
5.5	Noise simulations	44
5.6	Signal to noise ratio	46
5.6.1	Charge amplifier without compensation	47
6	Testing	48
6.1	Dynamic testing	50
7	Results	53
7.1	Testing known capacitors	54
7.2	Testing a parallel plate capacitor	54
7.2.1	Air gap between plates	55
7.2.2	A layer of new rubber between plates	55
7.2.3	A layer of worn rubber between plates	55
7.3	Testing wheel tire	56
7.3.1	Wheel with new tire between plates	56
7.3.2	Wheel with worn tire between plates	57
7.4	Dynamic testing	57
8	Conclusion	59
8.1	Recommendations	59

Appendices	61
A Python code	63
A.1 Current sensor plots	63
A.1.1 Linearity	63
A.1.2 Output voltage	65
A.1.3 Temperature	66
A.2 Simulation code	67
A.2.1 Ac sweeper main	67
A.2.2 Ac sweeper	69
A.2.3 Ac sweep parser	71
A.2.4 Noise main	72
A.3 Other plots	73
A.3.1 Tire harmonics	73
A.3.2 Permittivity	74
B Netlists	76
B.1 LF356	76
B.2 AD745	78
B.3 Charge amplifier with compensation	81
B.4 Charge amplifier without compensation	81
C Shell script	83

Preface

Every year, the Nuon Solar Team builds a new solar powered car. The team consists of 16 students, which hail from all different faculties at the Delft University of Technology. The car competes at the absolute top of its class and has won almost all races in Australia and South Africa since 2001. Needless to say, the team is driven to be the best and continuously looks to improve the performance of their car, Nuna. The ability to analyze currently unknown behaviour could help uncover where more performance enhancement is possible. However, this would require sensors around and in the car to collect this data. Since the team itself is working with limited time such projects are difficult to pursue, especially considering the required background knowledge in electronics, MCUs, software, etc. Due to these limitations, this project has been outsourced as a bachelor graduation project electrical engineering.

After initial talks with the Nuon Solar Team, it became clear that the priority was on the development of their own current sensor that is able to send its measurements over a CAN bus. As this was the highest priority, the group first collectively did a lot of research on various types of current sensing techniques. After this was done, the team split into subgroups which worked on isolated problems. This thesis will discuss Hall effect and magnetoresistive based current sensing, which are two of six current sensing techniques that were researched by the BAP group. Accuracy, power consumption, robustness and feasibility are all criteria that are discussed. It will become clear why Hall effect sensing is the most feasible of the two, and how it compares to shunt resistor based sensing.

The highest priority was put on the current sensor. Therefore, two of three subgroups combined their efforts to investigate this, while the other worked on a micro controller for analog to digital conversion and a CAN interface. Afterwards, the division of the subgroups became as follows:

- Subgroup 1: Shunt/amplifier current sensor
- Subgroup 2: Microcontroller with CAN interface
- Subgroup 3: Hall effect current sensor and tire wear sensor

The second part of this thesis will cover the continuation of an older bachelor graduation thesis from 2009 [1]. This thesis covered the monitoring of tire condition. Part of this thesis covered a capacitance based sensor, which could sense the thickness of the rubber tires by the change in capacitance. The Nuon Solar Team expressed great interest in further investigation of this topic, because the possibility to monitor tires while driving would be a great asset to the team.

Part I

Current sensor

Chapter 1

Introduction

Measuring current is of great importance in Nuna. Current measurement data is used during the race to determine the remaining energy in the batteries. This part will describe the background theory and feasibility of Hall effect and magnetoresistance based current sensors. After which, in chapter 4 it will become clear that a magnetoresistive based sensor is not feasible. A design is made for testing and measuring a Hall effect based sensor. The results are compared to a shunt resistor based current sensor. This investigation was done collectively with another subgroup.

1.1 Problem definition

Presently, the Nuon Solar Team uses Murata 1 m Ω base mounted shunt resistors [2] paired with a IMC μ -CANSAS differential voltage amplifier [3] for measuring current. This device is able to measure a differential voltage and send this value over a CAN bus to the central computer of Nuna. The current measurement system is presently comprised of shunt resistors at 3 different locations each paired with a CANSAS voltage amplifier. Figure 4.2 presents a simplified layout of the power system. The primary assignment of this part of the BAP is to design an alternative to this device. This task has been divided among subgroups as follows:

- One subgroup investigates the present way current is being measured, which is done using a shunt resistor. Also, they will be concerned with amplification of the small voltage which drops across the shunt resistor. This will involve designing and testing a differential amplifier which outputs an appropriate voltage that can be turned into a digital signal.
- This subgroup investigates an alternative method of current sensing. This will become clear in chapter 4, where both Hall effect sensing and magnetoresistive sensing are explored.
- The last subgroup will be concerned with programming a microcontroller, which will provide analog to digital conversion as well as the CAN interface.

1.2 Scope

The scope of the task will be further explored when listing the requirements in chapter 2. However, as the project progressed and tasks became clearer the groups would have their hands full on the assigned tasks. It should be noted that some parts of the respective subgroups' theses are shared, since some research was done collectively. The comparing and testing of the shunt based current sensor and Hall effect sensor used the same test setup for matching results.

Chapter 2

Requirements

This chapter describes the requirements associated with the design of the current sensor. A clear list of requirements was not provided directly by the Nuon Solar Team. These requirements were derived from driving conditions during races, as well as the current infrastructure of Nuna's current power system and electronics which devices are currently used in Nuna.

- Current measurements need to be communicated over a CAN bus
- A digital resolution of 1 mA
- Accuracy of at least 2.5 mA
- Robust design
- Relatively easy to replace
- Temperature operating range from 5-50 °C
- Must run off a 12 V dc power supply
- Power consumption should be as low as possible
- Weight must be kept to a minimum

It should be noted that some of these requirements are vague and open to interpretation, because values for "as low as possible" and "must be kept to a minimum" are not defined. Hence, requirements such as this are referred to the current system and to the judgement of the Nuon Solar Team. The team has expressed robustness as the top priority for electrical systems and thus this will be taken into account before weight and power consumption within reasonable bounds.

Chapter 3

Theoretical background

This chapter describes the underlying principles of magnetoresistive and hall effect current sensors. This information can be used to better understand the implementations of the respective current sensors.

3.1 Hall effect

When charged particles move through a magnetic and/or electric field, a force is exerted on them. This is the Lorentz force, described by equation 3.1. When the particles are bounded by a medium like a metal wire or plate, negative and positive charge will accumulate on opposite sides of the conductor. This separation of charge imposes a potential difference across the conductor, the Hall voltage. Figure 3.1 shows this principle.

Therefore, because every moving electrical charge produces a magnetic field, the Hall effect can be used to sense electrical current. A Hall element will require a small bias current through the Hall element. Once current is flowing through the Hall element, placing it in a magnetic field gives rise to the Hall voltage.

The brown copper plate in figure 3.1 is called the Hall element. This element is usually metal or a semiconductor material [4] [5]. A larger separation of charge will cause a high voltage across the element.

3.1.1 Open loop Hall sensors

Open loop Hall sensors use the Hall voltage to directly measure the current. The disadvantage of directly measuring the Hall voltage is saturation of the Hall element. This will cause the Hall voltage to no longer rise with increasing current, hence causing non-linearity [5] [6].

3.1.2 Closed loop Hall sensors

While open loop hall sensors are cheaper than their closed loop counterparts, they also suffer from more inaccuracy, a slower response and are more affected by electrical noise [7]. Closed loop Hall sensors use a secondary coil which is used to compensate the current in the primary. This compensation causes the total magnetic field measured by the hall sensor to be at a constant value, which helps with maintaining linearity. Thus the hall effect sensor in this case is not the main measurement device, but rather used as feedback. The actual measurement of the main current is done by measuring the current through the secondary coil which is related to the main current depending on the winding ratio. This current measurement is often done using a resistor and measuring the voltage drop. While this may seem similar to using a shunt, this technique offers galvanic isolation from the main current.

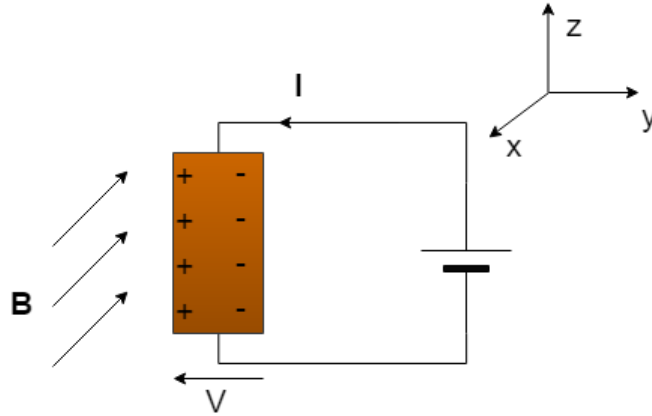


Figure 3.1: Graphical representation of the Hall voltage across a metal plate. The magnetic field \vec{B} is pointed in the $+\hat{x}$ direction.

$$\vec{F} = q(\vec{E} + \vec{v} \times \vec{B}) \quad (3.1)$$

3.2 Magnetoresistance

Magnetoresistance is the property of a material that its conductivity changes with an applied magnetic field. The discovery of the magnetoresistive effect dates back to 1856, when it was observed by Lord Kelvin [8]. For ferromagnets like iron, this property also depends on the direction of current flow in the material. Hence, similarly to the Hall effect, it can also be used for direction sensing [9].

Placing a magnetoresistive element next to a current carrying wire, changes its resistance based on the magnetic field produced by the current. By running a known bias current through the magnetoresistive element and measuring the voltage drop, the magnetic field strength can be determined. From the magnetic field strength, the current can be derived.

Magnetoresistive sensors are inherently non-linear [6] [10]. This can be compensated using a closed loop circuit, remaining in the linear region of the magnetoresistive element. This approach is similar to that use in closed loop Hall sensors.

3.3 Galvanic isolation

A Hall effect or magnetoresistive sensor has the benefit of the measurement circuit being galvanically isolated from the current being observed. When two electrical circuits are galvanically isolated no direct current can flow between them. However energy and information may still be transferred from one to the other. This is particularly useful in circuits where information transfer or energy transfer is needed, but whose grounds are at a different potential.

On top of that galvanic isolation is beneficial in cases where a measurement of a high power system is needed. The high power circuit will be isolated from the measurement circuit and thus possible high voltages will not be present in the low power measurement circuit. This improves safety and robustness of the system.

Chapter 4

Design

To better understand the problem a schematic of the power system of Nuna can be seen in figure 4.2. This image can also be found in the thesis of another subgroup who were concerned with the design and testing of the shunt based current sensor [11]. A schematic of the CANSAS can be found in figure 4.1. As figure 4.2 shows, the 3 locations current is measured at are:

- Battery
- MPPT ¹
- Motor

Each of these locations has a different associated current distribution. The Nuon Solar Team has provided us with data from a full race, with all measured currents. The current distribution for the battery, MPPT and motor can be found in figures 4.4, 4.5 and 4.3 respectively. Table 4.1

4.1 Coulomb counting

The most important location where current is measured is at the battery. The team uses this data to make predictions as to how much energy is remaining in the battery. Combined with weather data, a prediction is made as to how fast the car can drive without completely draining the battery before the race is over. Ideally, the battery should be completely drained just when the finish line is crossed. This way the maximum amount of available energy was used during the race. Energy entering the battery can be determined with the simple equation 4.1. “Coulomb counting” is essentially integrating current with respect to time, which is how the remaining charge in the battery is determined. Equation 4.2 shows this. Since a current is being integrated, white noise is not as relevant, because the average value is 0 and thus integration results in no error. Current offset however, will have an impact on the integrated value.

$$E_{battery} = E_{solar} - E_{motor} - E_{loss} \quad (4.1)$$

$$Q(t=0)_{battery} + \int_{t=0}^t I(t)_{battery} dt = Q(t)_{battery} \quad (4.2)$$

¹Maximum Power Point Tracker, used to maximize the output power of solar cells. For more information see: [12]

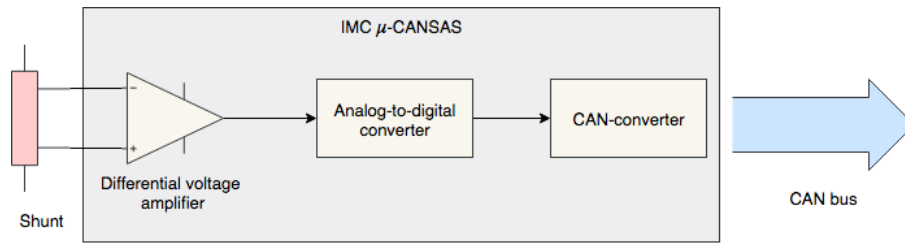


Figure 4.1: Diagram of the IMC μ-CANSAS

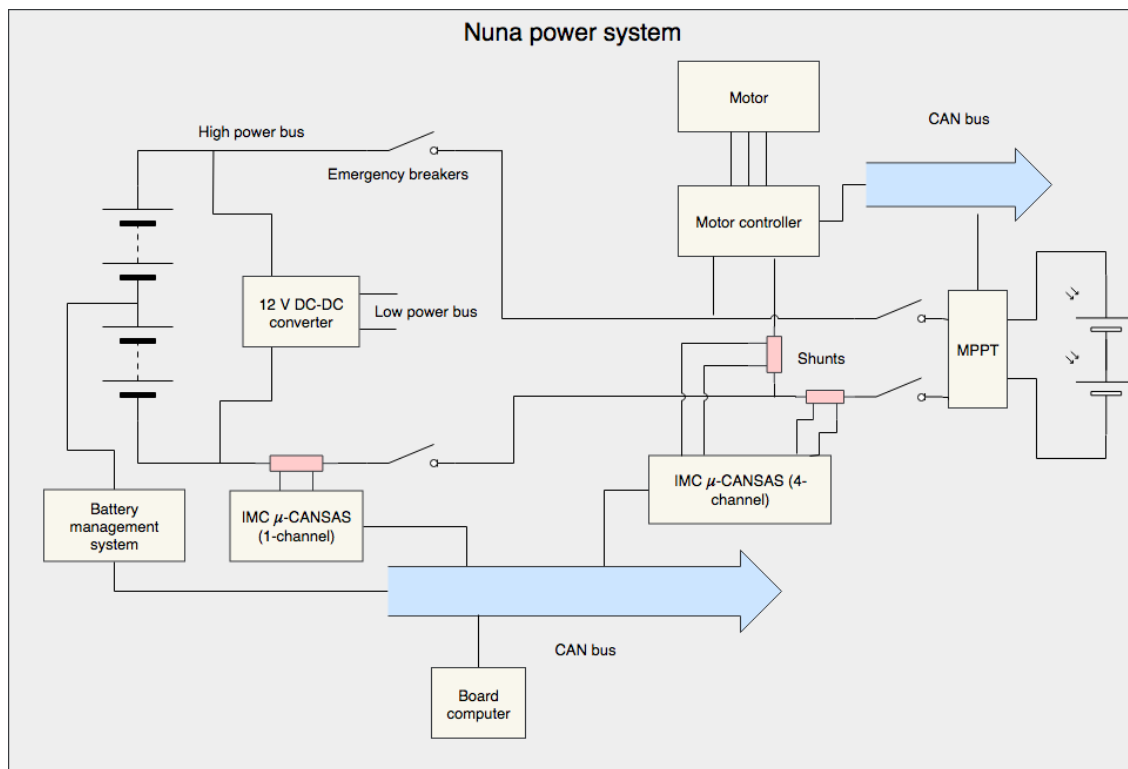


Figure 4.2: Diagram of the Nuna power system. This image was shared with another subgroup.

Current type	Mean	Max	Min	Std. dev.	Ratio
Battery	1.79	32.55	-29.43	4.40	78.14%
Motor	5.46	34.06	-27.20	4.25	76.21%
MPPT	3.89	9.79	-0.03	1.93	60.43%

Table 4.1: Table of current measurement properties. Ratio refers to the percentage of current measurements that fall within 1 standard deviation from the mean. All currents are listed in Ampere.

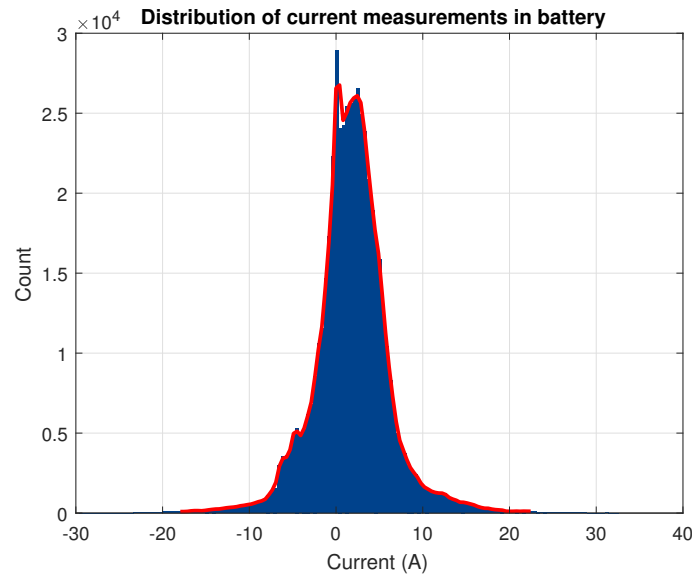


Figure 4.3: Plot of current distribution in the battery

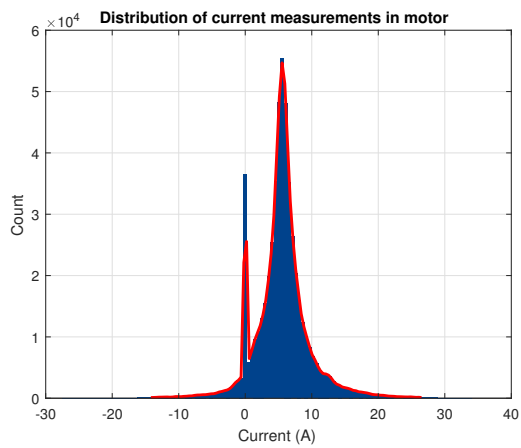


Figure 4.4: Current distribution in the motor

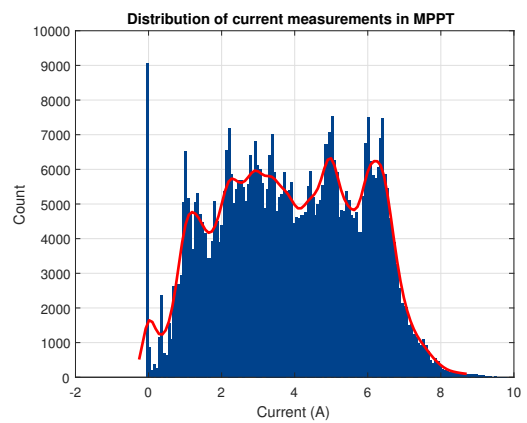


Figure 4.5: Current distribution in the MPPT

4.2 Temperature

Temperature measurements performed by the battery management system (BMS) were provided in the dataset as the current measurements. The battery is by racing regulations required to stay below a certain temperature, hence it needs continuous motoring. This is convenient, since it gives an indication as to what internal temperatures Nuna experiences. Aside from the data, the Nuon Solar Team has stated the internal temperature of Nuna can reach up to 50°C. Moreover, during races in South Africa, temperatures as low as 5 °C have been measured. The sensor must be able to withstand such temperatures. Table 4.2 shows more data on the measured temperatures of a race in Australia.

Temperature measurements	
Mean	33.61 °C
Min	20.64 °C
Max	42.58 °C
Std. Dev.	5.54 °C
Ratio	56%

Table 4.2: Temperature measurement statistics. Ratio refers to the percentage of measurements that fall within 1 standard deviation from the mean.

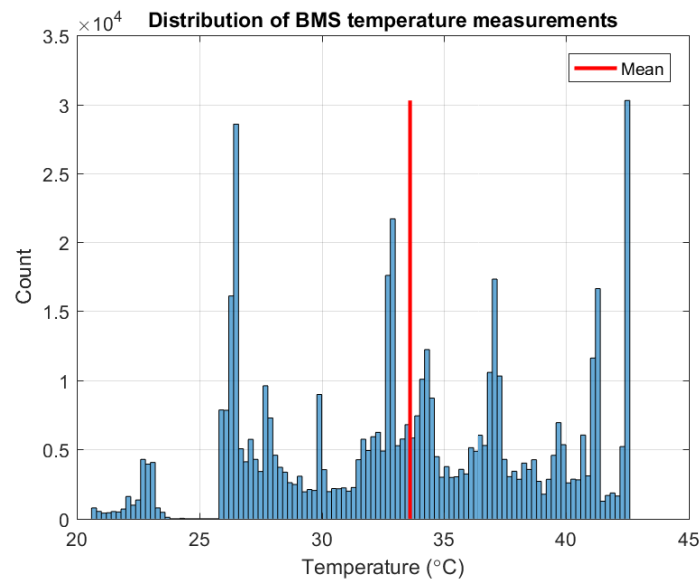


Figure 4.6: Distribution of temperature measured by the battery managements system (BMS).

4.3 Sensor comparison

Finding current transducers using the Hall effect to measure current was straight forward. They are widely available and table 4.3 shows a comparison between various types. The choice of magnetoresistive based sensors was very limited. Just one model manufactured by Sensitec [13] was found across various electronics distributors (farnell, rs-components and digikey). The datasheet showed an accuracy comparable to Hall effect sensors (0.5%-1%), and a slightly higher energy consumption. However, due to delivery constraints this sensor was deemed not feasible.

Manufacturer	Type	Max. current	Nominal accuracy	Power consumption estimate
LEM	LTSR 15-NP	48 A	0.2%	100 mW
LEM	LA 25-NP	36 A	0.5%	525 mW
LEM	H AIS 50-P	50 A	1%	100 mW
Multicomp	TH50A	50 A	1%	80 mW
Honeywell	CSLA2CD	72 A	2%	120-240 mW

Table 4.3: Comparison between various Hall effect sensors

4.4 LTSR 15-NP

Many Hall effect sensors on the market are especially made for high currents (100+ A) [14], but many models also introduce a lower current counterpart. The LEM LTSR 15-NP was eventually chosen for testing, since it combined the highest accuracy with the desired input current.

4.4.1 Internal circuit

The LTSR 15-NP is a closed loop Hall effect sensor. The datasheet of the LTSR 15-NP [15] provides a simplified version of the internal circuit. Figure 4.7 shows the circuit. The current to be measured runs through the primary coil, which generates a magnetic field in the transformer core. The Hall element resides perpendicular to the core. The Hall voltage is compensated by running a current through the secondary coil, which generates a magnetic field in opposite direction, cancelling the net magnetic field. This way, the Hall voltage is kept at 0, meaning the magnetic field in the Hall element will not saturate. The current through the secondary coil is measured and transformed to a voltage at the output.

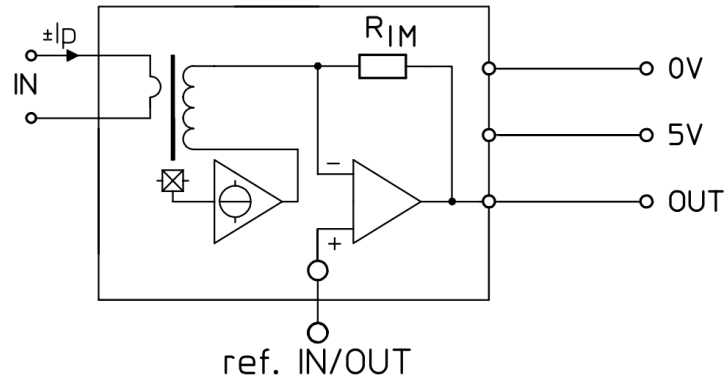


Figure 4.7: Simplified schematic showing the operating principle of the LTSR 15-NP. Source: [15]

Chapter 5

Testing

Datasheets only offer so much information about the actual current sensors. For an actual objective comparison the sensors are tested under conditions relevant to our case. In this case the effects of the following factors is investigated.

Testing the Hall effect sensor was done by creating a custom test setup. A copper laminated PCB was used as base. First, holes were drilled to accommodate the input and output leads of the sensor. After which holes were drilled to attach 6 mm² cables. Ring terminals were crimped to the cables to make them easily attachable with a bolt and nut. Additionally a small part of the PCB was removed to accommodate the output leads of the sensor's biasing and amplifier circuit. The designed test setup can be seen in figures 5.2 and 5.1.

The test setup can be seen in figure 5.4. The sensor was tested under varying conditions. Temperatures ranging from 0-50 °C. Currents ranging from -30 A to 30 A. The following equipment was used:

- Delta SM52-30 power supply, can provide currents up to 30 A
- Fluke t3000 FC thermometer
- Fluke 177 multimeter for voltage measurements
- Delta 5 V power supply for the biasing and amplifier circuit
- Heat gun
- Coolant spray

Since the sensor is quite large, it is more difficult to homogeneously cool or heat. To ensure the whole sensor was at an equal temperature, the temperature probe was pressed against the middle of the sensor. This is shown in figure 5.3. As soon as the temperature was observed to decrease, the measurement was noted. The ambient temperature was also noted.

The output voltage is measured across the blue and green wires, which are output voltage and reference voltage respectively. The reference voltage is kept at 1/2 times the supply voltage, and provides a reference point to bias the output voltage to 0 V when no current is flowing through the sensor, i.e. the voltage across the reference and output wires is 0 V at 0 A, 2.5 V at 50 A and -2.5 V at -50 A.

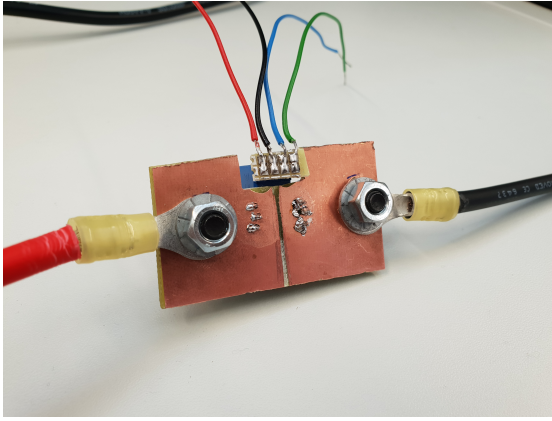


Figure 5.1: Bottom of the test board

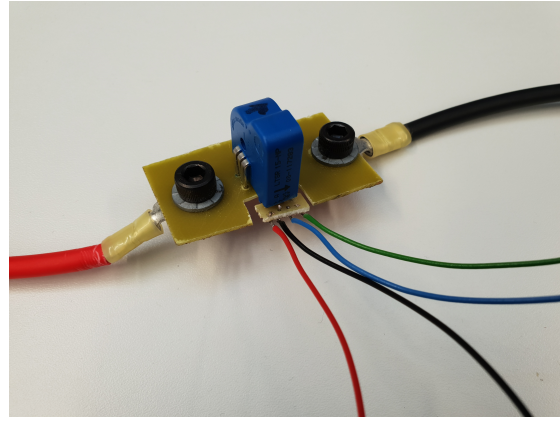


Figure 5.2: Top of the test board

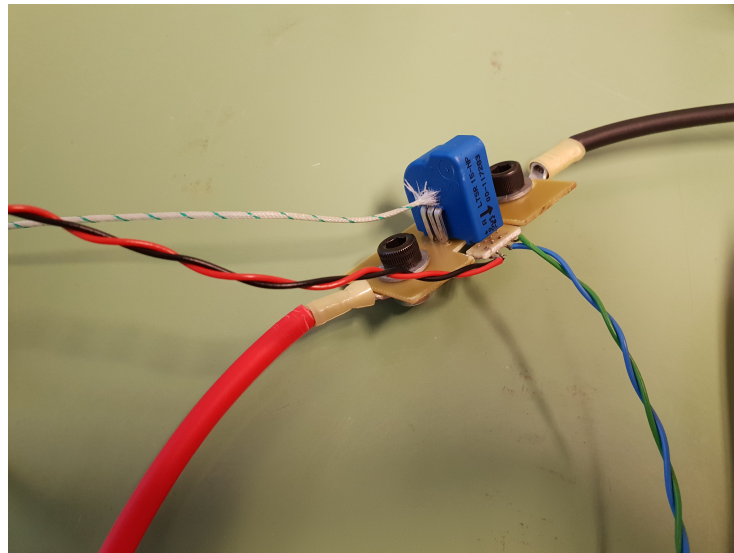


Figure 5.3: LTRS15NP with temperature probe

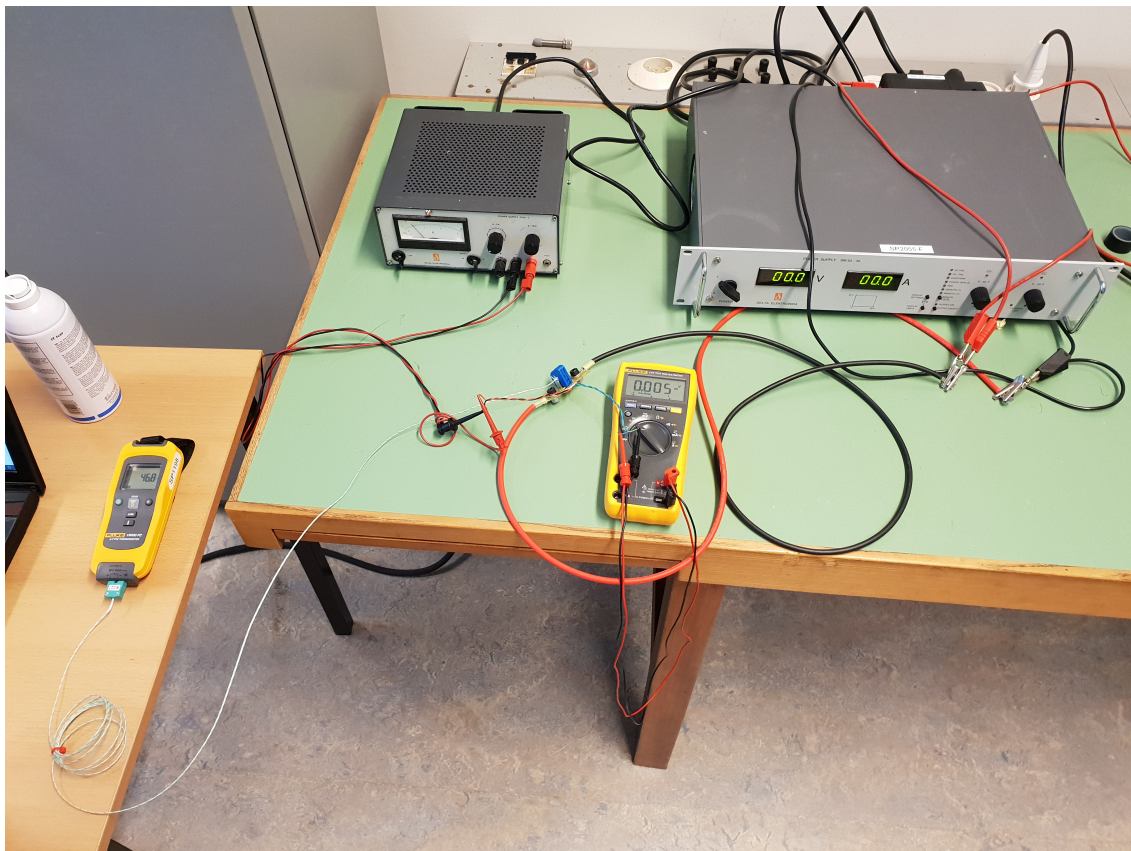


Figure 5.4: Full test setup for the LTSR15NP

Chapter 6

Results

In this chapter the measurement results are presented. Plots have been made of the output voltage with respect to current and offset voltage with respect to temperature. From this data the temperature offset and linearity of the sensor are deduced.

Figure 6.1 shows the output of the LTSR-15NP at currents ranging from -30 A to 30 A. These currents are representative of what the sensor would experience in Nuna. The temperature change was also measured for the positive currents. Since the direction of current is irrelevant to the heating of the sensor. Under full load, the sensor was heating to up to 30°C. For positive currents, the measurements were performed every 15 seconds, with increments of 1 A. For negative currents, measurements were performed with increments of 5 A. According to the datasheet [15], the output sensitivity is 41.6 mV/A. This value can be found in table 6.1 among others.

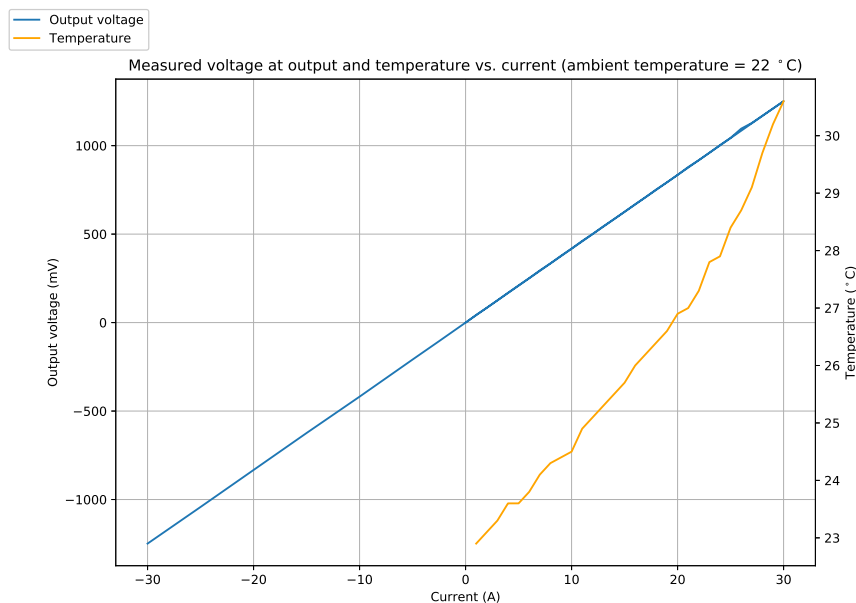


Figure 6.1: Plot of output voltage measurements vs. input current, and the temperature of the sensor as the measurements were performed

Sensor	Sensitivity	Mean temperature offset	Mean linearity error	Mean temp. linearity error
LTSR15NP	41.9 mV/A	0.157 mV/°C	1.092 mV	0.255 mV
Shunt/MAX4238	55 mV/A	0.0085 mV/°C	1.564 mV	0.214 mV

Table 6.1: LTSR-15NP and shunt/MAX4238 characteristics derived from measurements

6.1 Linearity

Linearity was also tested by calculating the absolute error from a true line. This was done by fitting a line in the data using the method of least squares in the numpy library. Then, the error was calculated according to equation 6.2. As can be seen in table 6.1, the mean error was calculated to be 1.092 mV. This is a significant part of the 41.9 mV/A output sensitivity. The exact value is calculated in equation 6.1.

$$\text{Average current error} = \frac{1.092}{41.9} = 26.06 \text{ mA} \quad (6.1)$$

$$\text{Error} = |\text{measured data} - \text{fitted line}| \quad (6.2)$$

6.2 Temperature offset

Being a Hall effect based current sensor, the LTSR-15NP experiences some thermal voltage offset. This was measured in the test environment using a heat gun and cooling spray, as described in chapter 5. Figure 6.3 shows the effects from cooling and heating the sensor on the offset voltage. The sensor exhibits nonlinear temperature offset, which makes compensating difficult.

6.3 Noise sources

During testing, additional noise sources were uncovered. Electromagnetic interference was tested, and an unpredictable offset problem caused by an unknown source was observed.

6.3.1 Electromagnetic interference

In the Nuna, cables carrying currents up to 35 A produce electromagnetic fields in the car. These fields could interfere with the accuracy of the Hall effect sensor. This was tested by running up to 30 A through cables and placing the Hall sensor at various distances from the wires. No change in output voltage could be observed when the test were done.

6.3.2 Unpredictable offset problems

During testing, the LTSR15NP was observed to have an unpredictable offset while being at room temperature. This offset was observed to change by up to 2 mV as time passed. No current was running though the sensor at the time. It has remained unclear as to what causes this offset, but it is a problem that should be kept in mind.

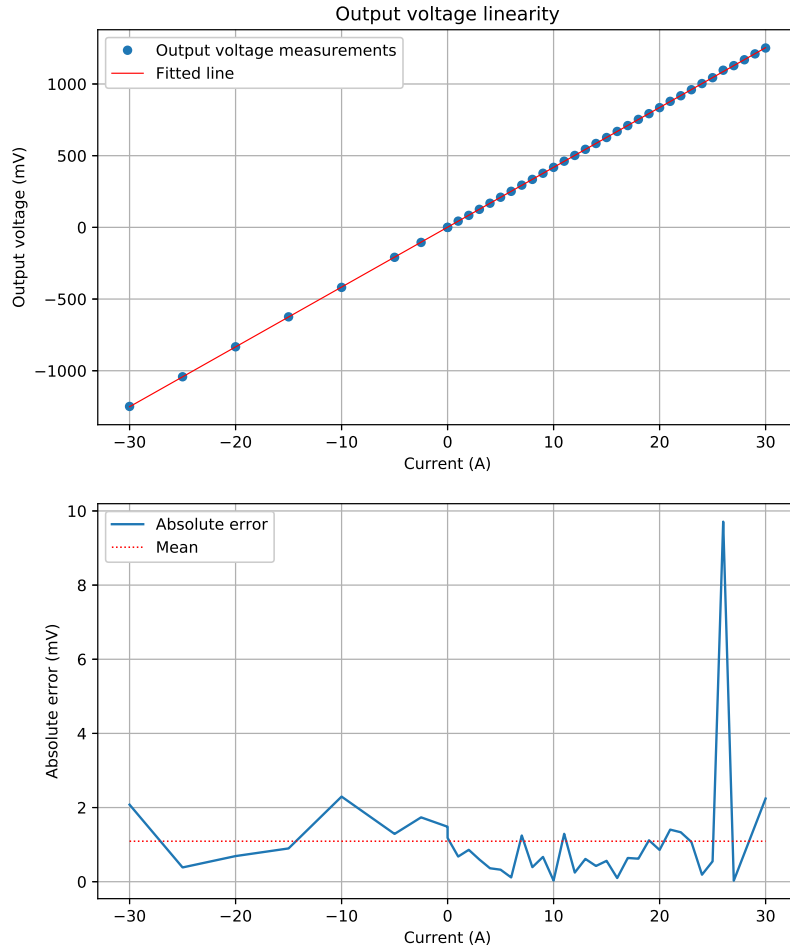


Figure 6.2: Plot of measurements linearity. The mean absolute error is 1.092 mV

6.3.3 Questionable robustness

During testing, a LTSR15NP broke due to unknown reasons. The output voltage became much less linear and the sensitivity of 41.6 mV/A plummeted. An attempt to reproduce this behaviour on a new sensor failed, but it did require an additional sensor to be purchased.

6.4 Comparison to shunt

The shunt uses an external amplifier for measuring the voltage across the shunt, which was a MAX4238 in differential configuration [16] during testing. The circuits can be found in the thesis of the other sub-group [11]. The shunt was observed to be more stable under changing temperature. The output voltage of the shunt amplifier was not observed to change much less when cooled and heated as shown in figure 6.4. However these measurements will probably need to be performed using a higher resolution voltage

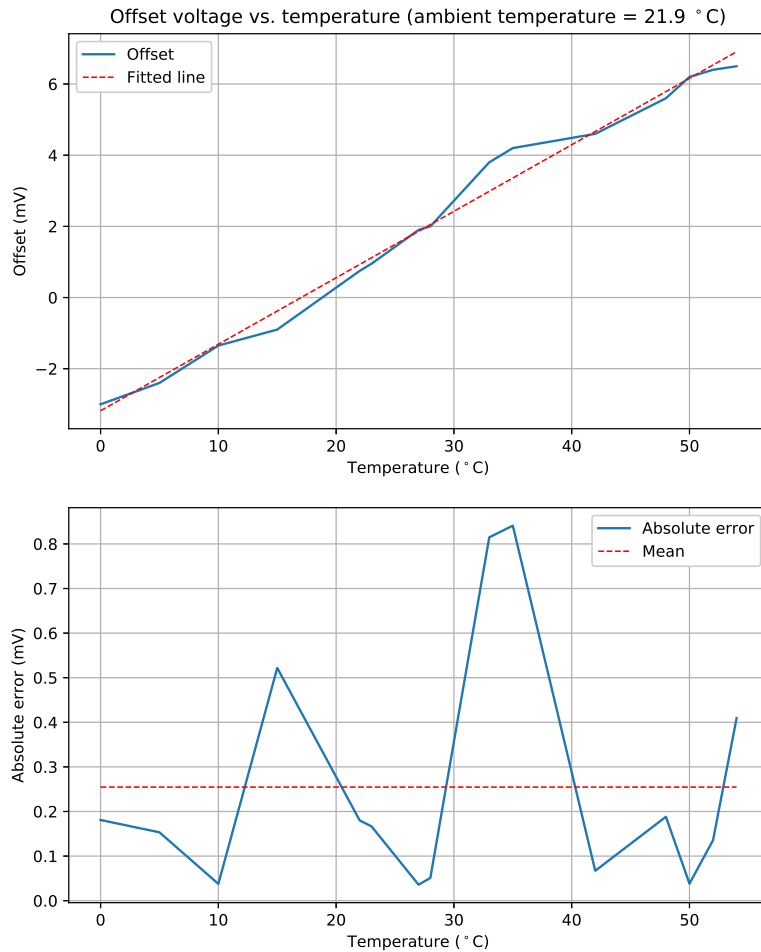


Figure 6.3: Plot of measurements

measurement for more accurate results. Current measurements and linearity error are shown in figure 6.5. Also, the temperature of the amplifier itself was not observed to change more than 0.1 °C during current measurements. The mean linearity offset was measured to be 1.56 mV. On a output sensitivity of 55 mV/A, this results in a error current of 28 mA, which is slightly higher than the Hall sensor. However, the other subgroup has determined a new op amp to lower this number. Temperature drift was found to be 0.0085 mV/°C, which is much lower than the Hall sensor. The mean temperature linearity was also found to be lower, at 0.214 mV. All values can be found in table 6.1

6.4.1 Power consumption

The sensor in standard configuration has an internal resistance of 0.18 mΩ, this is 0.82 mΩ less than the resistance of the shunt. However, the LTSR15NP requires a 5 V source for its biasing and amplifier circuit, which draws 20 mA nominally. The shunt voltage also needs amplification, of which the power consumption is not yet known. The difference in power consumption between the shunt with amplifier and

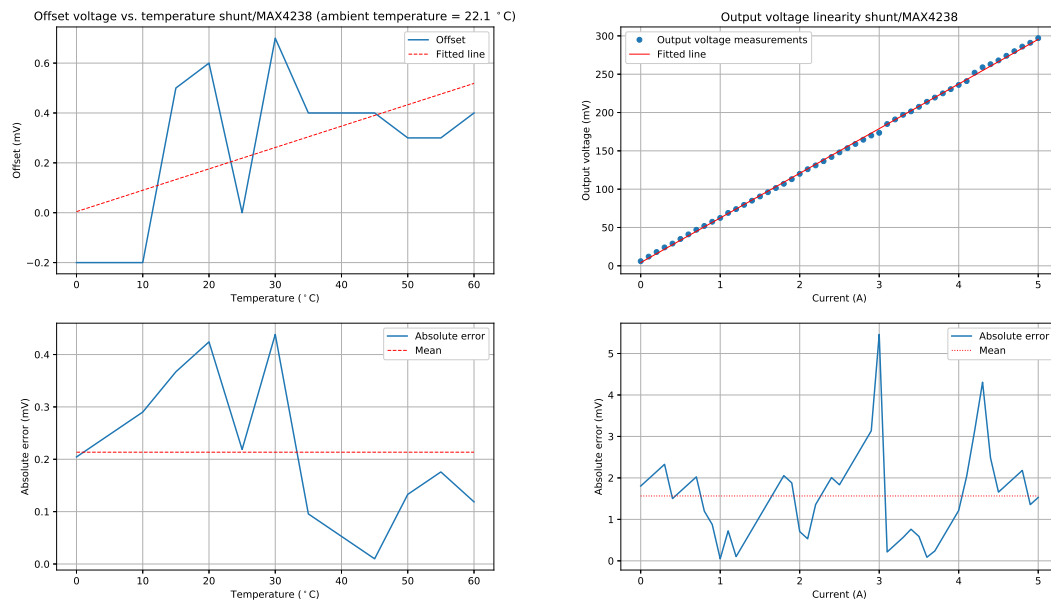


Figure 6.4: Shunt temperature measurements. Mea-Figure 6.5: Shunt linearity measurements. Measurement were performed by the other subgroup [11]ment were performed by the other subgroup [11]

LTSR15NP (Hall) can be found using equation 6.3.

$$\Delta P = R_{Hall} I_{avg}^2 + I_{bias} V_{source} - (R_{shunt} I_{avg}^2 + P_{amp}) \quad (6.3)$$

Chapter 7

Conclusion

During testing of the Hall effect sensor, it became clear that the required accuracy could not be achieved. It was calculated that the sensor has up to 26 mA error current from non-linearity. This is over 10 times greater than the required 2.5 mA accuracy. Temperature offset also proved a problem, which was measured to be 0.157 mV/°C and an average linearity error of 0.255 mV. This makes compensating for temperature difficult.

The linearity current error of the shunt and Hall sensor were similar, 26 mA and 28 mA for the Hall and shunt respectively. But temperature drift of the shunt was much lower, at 0.0085 mV/°C compared to 0.157 mV/°C. The mean temperature linearity error was also found to be 0.41 mV lower for the shunt. Therefore, for the best stability and robustness the shunt resistor based current sensor is recommended. This is also corroborated by a Hall effect sensor breaking during testing, which makes it more difficult to recommend due to robustness being a top priority on Nuna's agenda.

Another advantage to using the shunt/amplifier combination, is that individual components can be tweaked and replaced with relative ease. With the Hall sensor this is not possible, since the amplifier circuit is embedded in the sensor package. A broken amplifier would mean having to replace the whole sensor, which is more expensive and time consuming than replacing a socketed IC. Only if galvanic isolation is greatly desired, a Hall effect sensor should be considered.

7.1 Further work

To make a more accurate comparison between the shunt/amplifier combination and the Hall effect sensor additional tests should be done. The temperature dependence of the shunt itself was not properly measured, only of the amplifier. To measure temperature dependence more accurately, the temperature should be kept stable for several minutes, ensuring the object to be measured is completely at the specified temperature. Also, the temperature offset measurements of the amplifier should be done using a higher resolution voltmeter, since a resolution of only 0.1 mV could be achieved using the multimeter. Several improvements will be made to the shunt/amplifier circuit, which can be found in [11].

Part II

Tire wear sensor

Chapter 1

Introduction

One of the most important factors in the NUNA both for drive performance and safety is the condition of the tires. During driving the tires get worn down over time. When the tire gets thinner it is more likely to burst which could cause the car to crash. Not only does this cause danger to the driver, it also causes a lot of time loss during the race. On the other hand, there have also been a few occasions in the past where the driver thought the tire had either burst or had worn away enough to warrant a change. When the car stopped to check whether it had, the tire seemed fine and the only thing that had chipped away was more time.

Every contestant participating in the WCS (World Solar Challenge) must abide to strict regulations [17]. One of which is that the car must stop for 30 minutes at designated control stops along the route. These stops are meant for switching drivers and visually inspecting the car. During this time the car may reconfigure itself, but the team is not allowed to touch the car in any way. The wheels of Nuna are almost fully enclosed in wheel covers, which are placed for air drag reduction. These covers have very little tolerance, as there is only 7 mm of space between the wheel and the wheel covers. This in combination with low ground clearance and the regulations makes the tires difficult to inspect manually.

To prevent the negative effects of the wearing out of the tires, tires are already replaced every day. This may seem sufficient, however external factors such as wind speeds play a huge role on the rate at which tires wear down. During some conditions a tire may need replacement after only 15 minutes. Under extreme testing conditions the tires can be worn down in as few as 8 minutes.

Due to all aforementioned problems, real-time tracking of the tire thickness during driving would be of great benefit to the Nuon Solar Team. This part is a continuation on an old bachelor graduation project from 2009 [1], where a similar approach to measuring tire thickness showed promising results. The following chapters will outline how by measuring a change in capacitance the tire thickness is measured.

Chapter 2

Requirements

This chapter describes the requirements associated with the design of the tire wear sensor. A clear list of requirements were not provided directly by the Nuon Solar Team. These requirements were derived mostly from another graduation project [1] as well as from various conversations with Nuna and other subgroups in this project.

- Output should be in the 0 to 5 V range
- 5 levels of tire wear should be able to be distinguished
- Robust design
- Relatively easy to replace
- Temperature operating range from 5-50 °C
- Must run off a 12 V dc power supply
- Weight must be kept to a minimum

Chapter 3

Theoretical background

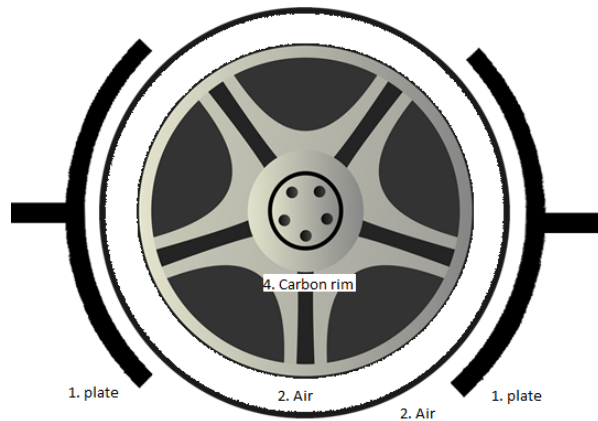
This chapter deals with the theoretical background of measuring tire thickness. In the other graduation project various options are considered [1]. It was concluded that measuring capacitance was the best option to determine rubber thickness. In this chapter this is worked out in more details. While current technology in for example image recognition has greatly improved, due to complexity and time pressure this is not considered in this thesis.

3.1 Capacitance

Capacitance is the ratio of the change in an electric charge in a system to the corresponding change in its electric potential. Any two adjacent conductors with a certain dielectric between them can function as a capacitor. The resistance encountered when forming an electric field, called permittivity, of the material(s) between the conductors is a factor that affects the value of the capacitors capacitance. Permittivity is often expressed in relative terms: $\epsilon = \epsilon_0 \cdot \epsilon_r$ where $\epsilon_0 \approx 8.85 \cdot 10^{-12} \text{F} \cdot \text{m}^{-1}$ is the permittivity of a vacuum and ϵ_r is the relative permittivity of a certain material compared to vacuum. Rubber has a relative permittivity of $\epsilon_r \approx 3$ to 7 while air has $\epsilon_r \approx 1$.

3.2 Wheel capacitance model

The wheel capacitance model is formed by two plates which both form a capacitor with the conduction carbon rim. The plate and rim in both cases are separated by a layer of rubber and 2 layers of air; one in the tire and one outside. This model is illustrated below.

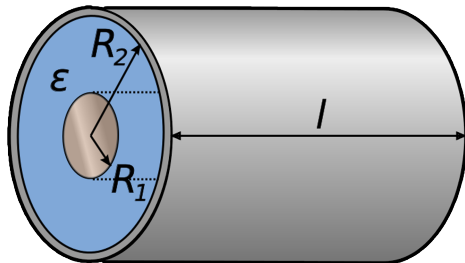


In the plate-wheel-system the following materials are identified:

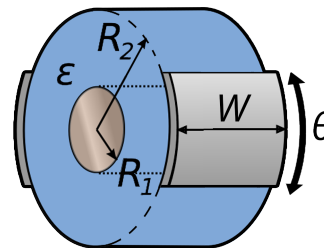
- 1. Plate (metal)
- 2. Air $\epsilon_r = 1$
- 3. Rubber $\epsilon_r = 3 - 7$
- 4. Carbon fibre $R_{edgetoedge} = 10\Omega$

To estimate the value of capacitance of a system, various equations exist. In this case, the wheel capacitance model is most comparable to that of a coaxial cable. The capacitance of a coaxial cable is given by equation 3.1, where

- C is the capacitance in F
- ϵ_r is relative static permittivity
- ϵ_0 is the electric constant ($\epsilon_0 \approx 8.854 \cdot 10^{-12} \text{ F}\cdot\text{m}^{-1}$)
- l is the length of the cable in m
- R_2 is the radius of the outer "plate" in m
- R_1 is the radius of the inner "plate" in m



$$C = \frac{2\pi\epsilon_r\epsilon_0 l}{\ln(R_2/R_1)} \quad (3.1)$$



$$C = \frac{\theta}{360} \frac{2\pi\epsilon_r\epsilon_0 w}{\ln(R_2/R_1)} \quad (3.2)$$

Equation 3.1 can be rewritten to approximate the wheel capacitance model by multiplying by the percentage of degrees the curved plates span the rim. This leads to equation 3.2, where

- C is the capacitance in F
- θ is the angle of the plate in degrees
- ϵ_r is relative static permittivity
- ϵ_0 is the electric constant ($\epsilon_0 \approx 8.854 \cdot 10^{-12} \text{ F}\cdot\text{m}^{-1}$)
- w is the width of the plate in m
- R_2 is the radius of the outer "plate" in m
- R_1 is the radius of the inner "plate" in m

While equation 3.2 may yield a good estimation of capacitance, it should be noted that fringing effects are ignored. In this case since the distance between two plates is large compared to that of an average capacitor,

parameter	description	value
d	distance between rim to plate	0.065 m
d_t	tire thickness	0.004-0.005 m
d_a	total distance of air	0.061-0.060 m
ε_{rubber}	relative permittivity of rubber	5
ε_{air}	relative permittivity of rubber	1
ε_{new}	relative permittivity of new tire	1.308
ε_{worn}	relative permittivity of worn tire	1.246
$\Delta\varepsilon_r$	relative permittivity difference	0.062
$\% \Delta\varepsilon_r$	% permittivity difference	4.71%

Table 3.1: Table showing values corresponding to calculation of relative permittivity

parameter	description	value
θ	plate span	60 °
ε_{new}	relative permittivity of new tire	1.308
ε_{worn}	relative permittivity of worn tire	1.246
ε_0	the electric constant	$8.854 \cdot 10^{-12}$
w	plate width	0.070 m
R_2	radius outer plate	0.275 m
R_1	radius inner plate	0.210 m
C_{new}	capacitance of new tire	3.147 pF
C_{old}	capacitance of old tire	2.999 pF
ΔC	difference in capacitance	0.148 pF
$\% \Delta C$	% difference in capacitance	4.71%

Table 3.2: Table showing values corresponding to calculation of capacity

fringing effects will play a large role [18]. Due to this, the estimated value will most likely be lower than the real value.

The distance from the rim of the wheel to the edge of tire is about 6 cm, so conducting plates can be placed at about 6.5 cm from the edge of the rim. The radius of the rim is about 21 cm. This yields $R_1 = 0.21$ m and $R_2 = 0.275$ m. A single plate spans about $\theta = 60^\circ$ and has width of $W = 0.07$ m. By definition the electric constant ($\varepsilon_0 \approx 8.854 \cdot 10^{-12}$ F·m⁻¹).

That leaves ε_r . The change in measured capacitance ΔC , in equation 3.2 is caused by a change in ε_r . ε_r depends on all the materials between the two conductors, which ideally would only be a layer of air, the layer of the tire consisting of rubber, and another layer of air inside the tire. The total distance from rim to plate is $d = 0.065$ m. Tire thickness is $d_t = 0.005$ m for new tires and $d_t = 0.004$ m for worn tires. This leaves 2 layers of air which when combined is between $d_a = d - d_t = 0.060$ m and $d_a = d - d_t = 0.061$ m. Since ε_r for rubber changes with frequency, an average value of 5 is used. Using equation 3.3 the relative permittivity of the combined layers is calculated. The results are listed in table 3.1. Using these values with equation 3.2, yields values as shown in table 3.2.

$$\varepsilon_r = \frac{d_{air}}{d} \varepsilon_{air} + \frac{d_{rubber}}{d} \varepsilon_{rubber} \quad (3.3)$$

As seen in table 3.2, the change amount of capacitance that needs to be measured is rather small. Having two of these capacitors in series, which the actual model consists of halves this value. While this means the combined capacitance would have value ranging from 1.574 to 1.500 pF, the percentage of change still equals 4.7%, which is measurable. The model is shown in figure 3.1, with C_3 the combined capacitance and R the resistance of the rim from plate to plate, $R = 10\Omega$. This means to be able to distinguish 5 levels a difference of $\Delta C = 0.0148$ pF needs to be able to be measured and a percentage difference of 0.94%.

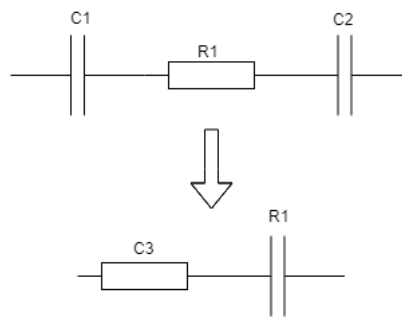


Figure 3.1: Model for wheel

3.3 Measuring capacitance

In this section three options of determining the capacitance change are discussed. The first two options come down to amplitude modulation of a known carrier wave, while the second makes use of frequency to carry information about the state of the tires.

3.3.1 Current measurement through capacitor

Perhaps the most simple way to determine capacitance is to put an alternating voltage across a capacitor and measure the amplitude its current. This requires small changes of current to be accurately measured. The amplitude modulated signal can be decoded by a rectifier, which yields a steady DC voltage signal. Due to its simplicity and promising results from the other thesis [1], this is option is preferred.

3.3.2 Measuring permittivity difference of rubber for different frequencies

The capacitance of the wheel-plate-system is frequency dependent. This is due to the relative permittivity of rubber, ϵ_r being frequency dependent. When a current consisting of two frequencies passes through the wheel-plate-system both frequencies will undergo a different value of capacitance. When the difference in capacitance in both these frequencies is measured the relative permittivity of the capacitors can be calculated. Since the permittivity of air is not frequency dependent and rubbers is, the difference in permittivity for two frequencies can be used as a measure for the thickness of the tire. While this option may be more resilient to dirt on the tires and changes in relative permittivity of air, it also considerably increases complexity because two waves forms need to be used. Considering the limited time available for this project in depth analysis and design of this option is not dealt with in this report.

3.3.3 Frequency measurement of oscillator

This option makes use of the capacitance of the wheel to form an oscillator circuit. The frequency at which the circuit oscillates can be measured and from it the value of capacitance can be determined. Like the previous option, this will be considerably more complex than the first option. On top of that, it also requires more complex circuitry to decode a frequency modulated signal. Due to this, in this report this option is also not dealt with.

3.4 Permittivity

Permittivity of various materials is affected by frequency, humidity and/or temperature. Since the capacitance measurement relies on higher permittivity of rubber than other media between the plates, knowing how the permittivity of these materials may change is of great importance.

3.4.1 Rubber

Rubbers permittivity is highly dependent on the frequency that is applied to the capacitor [19], ranging from 7 at 100 Hz to 3 at 1 MHz, as can be seen in figure 3.2. A high permittivity of rubber is preferred, since this means the overall capacitance will be larger, which makes measurement easier. On top of that a higher permittivity means the system will be more resilient to possible changes in permittivity of air.

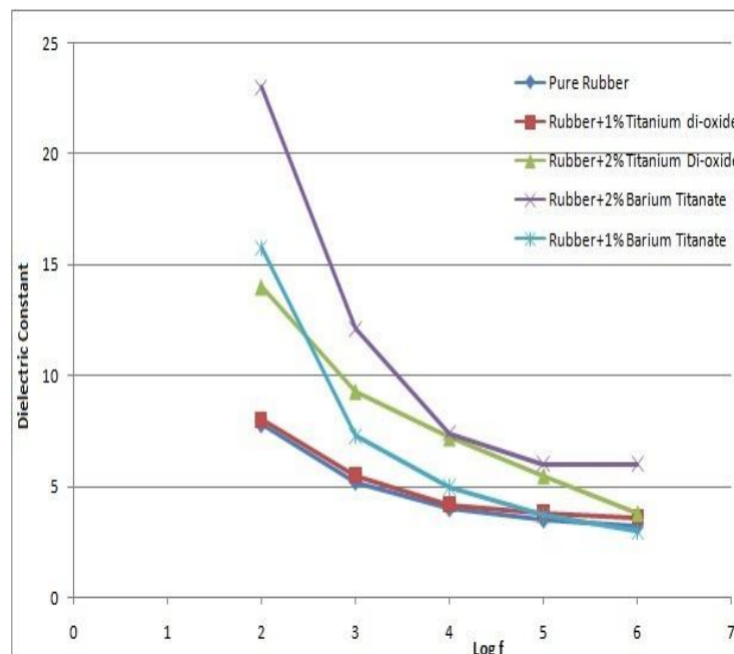


Figure 3.2: Dependence of rubbers permittivity on frequency

The same paper also discusses the effect of temperature on rubbers permittivity and this poses a potential problem [19]. When a 1 kHz frequency is used, at a temperature of 35°C a relative permittivity of 5 is measured, while at 95°C a relative permittivity of 10 is measured. A study on tire temperature at different speeds found that the temperature of rubber tires indeed is capable of ranging more than 60°C [20]. In some tires the temperature built to 140°C when driving at a speed 120 km/h. To counter this problem, temperature compensation may be needed. Proposed solutions to this problem include implementing an infra red thermometer to measure temperature of the tires and compensate by using a microcontroller. This however will be investigated in depth after rubber thickness can be accurately measured at a steady temperature.

3.4.2 Air

Unlike rubber, air's permittivity is independent on frequency, which is desirable. Effects on humidity and temperature however does vary. A paper discussing the effect of humidity on air-gap capacitors found that for ranges of humidity from 35% to 75% that percentage change of capacitance had a maximum of only

0.03 % when compared to dry air [21]. The same paper also compares the results of different levels of humidity at different temperatures. It finds that humidity and temperature have an independent effect on permittivity. The rate at which permittivity is affected by temperature is found to be even lower at 0.004%.

Chapter 4

Design

This chapter deals with the design of the circuitry needed to accurately measure a small difference of capacitance. It starts with a simple current to voltage amplifier and builds into a circuit capable of presenting a 0 to 5 voltage level to the microcontroller, based on the state of the tires. It uses a 12V DC supply to operate and makes use of a AC wave signal produced by the same microcontroller.

4.1 Measuring current through a capacitor

To measure the current through the wheel-plate-capacitor when a voltage is applied a transimpedance amplifier can be used. The most basic transimpedance amplifier using a feedback resistor, R_f and an ideal operational amplifier is shown in figure 4.1.

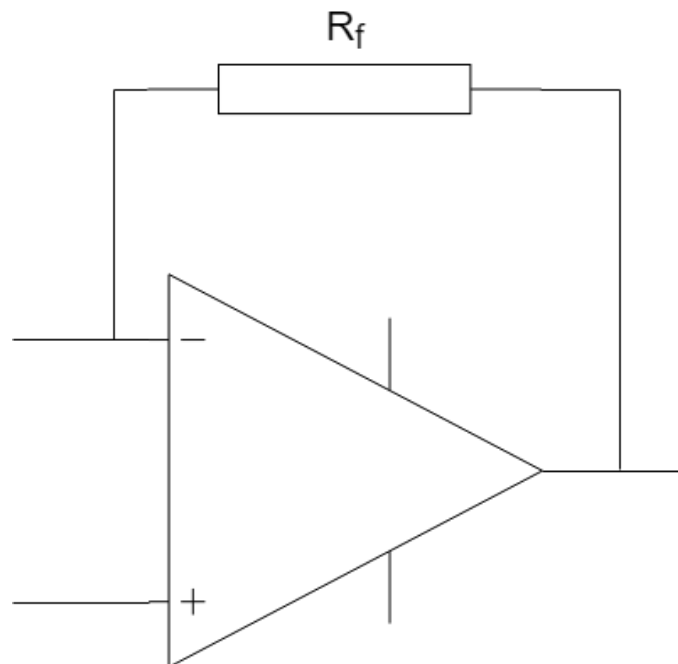


Figure 4.1: Transimpedance amplifier

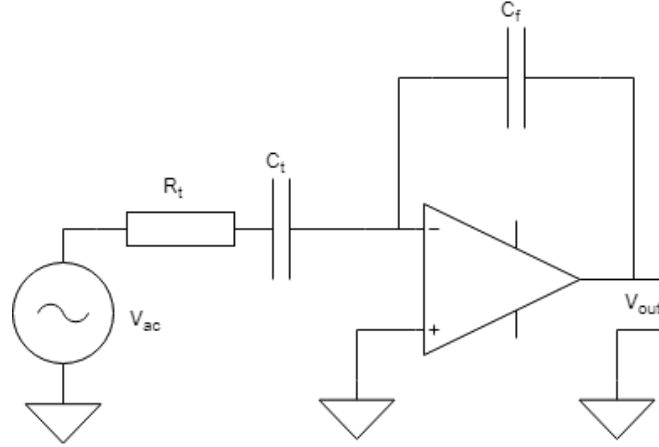


Figure 4.2: Ideal charge amplifier circuit with wheel model attached

However since in this case we are interested only in an alternating current signal of a chosen frequency, this resistor can be replaced by a capacitor. Using a capacitor as feedback produces less noise and changes amplifier type to that of a current integrator. Since integrating current over time yields charge and the output will be a voltage, this amplifier is also known as a charge amplifier or a charge-to-voltage converter. The ideal circuit is shown in figure 4.2.

In practise however operational amplifier are not ideal. They have finite open-loop gain, an offset voltage and input bias currents. When taking this into consideration several potential problems can be seen. Firstly, for DC the feedback capacitor acts as an open circuit, which means any DC-signals on the inputs of the op amp will amplified with the open-loop gain of the op amp. This is exactly what will happen due to the offset voltages and bias currents non-ideal op amps possess at the input terminals. To counter this effect a large feedback resistor, R_f may be added in parallel with the feedback capacitor, C_f . This limits DC gain. A second problem are the input bias currents, or rather the voltages they create at the input terminals of the op amp. Input bias currents are typically the same for positive and the negative terminal. In a circuit as depicted in figure 4.2 at the positive input of the op amp the input bias current will not produce a different voltage because of the connection to ground. However on the negative input the bias current will flow through the wheel resistance and capacitance, R_t and C_t and through the feedback network. This will cause a non-zero voltage at the inverting input and thus a voltage difference between positive and negative input, which will be amplified. To counter act this input on the negative input, that same impedance network can be connected to the positive input. Because bias currents at the positive and negative inputs are the same, the impedance network will create the same voltage at both inputs and thus no voltage difference. The charge amplifier circuit with a feedback resistor and a matching impedance network added is shown in figure 4.3, with $R_b//C_b = (R_t + C_t)//R_f//C_f$. The compensation impedance network may or may not be beneficial, depending on the bias current values of the particular op amp. If bias currents are low adding this compensation may add more noise than it will cancel. Since the compensation also shouldn't change the transfer function of the circuit it will be left out for now. Its usefulness will be discussed in chapter 5 simulation.

The transfer function of circuit depicted in figure 4.3 is given by equation 4.1, with V_{ac} used as input voltage, V_{in} .

$$\frac{V_{out}}{V_{ac}} = H(s) = \frac{-s}{s^2 R_t C_f + s \left(\frac{R_t}{R_f} + \frac{C_f}{C_t} \right) + \frac{1}{R_f C_t}} \quad (4.1)$$

When this equation is further analyzed a general bode plot can be drawn. The equation consists of 4 variables; two resistors, R_t and R_f and two capacitors, C_t and C_f . R_t and C_t comprise the wheel-system

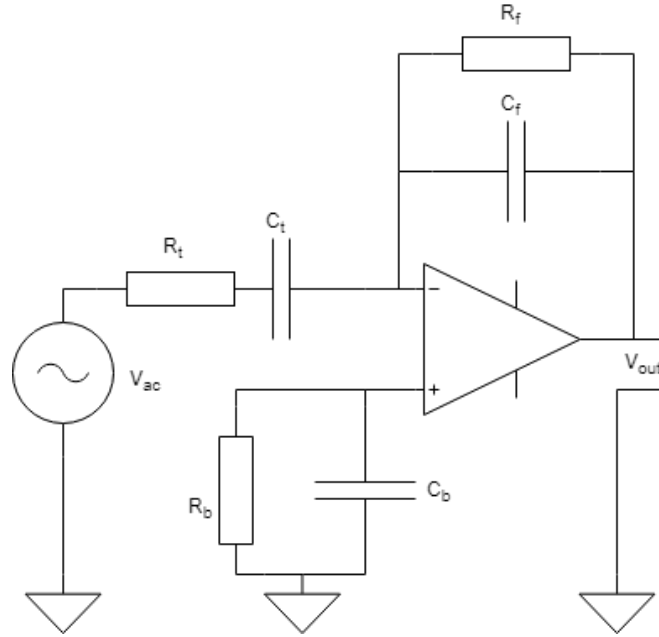


Figure 4.3: Charge amplifier circuit with added feedback resistor and bias current compensation

Component	Rough value
R_t	$10^1 \Omega$
C_t	10^{-12} F
R_f	$10^6 \Omega$
C_f	10^{-12} F

Table 4.1: Rough values of components

and their values are estimated to be $R_t = 10 \Omega$ and $C_t = 3.5 \cdot 10^{-12}$. The values of the other components can be chosen to be anything, however keeping the purpose of the circuit in mind, rough estimates of what their value should be can be deduced. Firstly, R_f . This feedback resistors should be large since for AC the current should flow through the feedback capacitor, C_f instead of R_f . The resistors purpose is to limit DC gain. This means R_f will in region of mega Ω ($10^6 \Omega$). For, feedback capacitor, C_f a value of capacitance is desired that leads to the large gain. A large gain is desired because small capacitor values need to be measured and the maximum gain of the circuit is almost exclusively dependent on the ratio $\frac{C_t}{C_f}$. Because of this, feedback capacitor C_f would ideally be chosen very small (in the region of 10^{-12} Farads). The rough values of the components are listed in the table 4.1.

Rewriting equation 4.1 to proper form yields equation 4.2.

$$\frac{V_{out}}{V_{ac}} = H(s) = -R_f C_t \frac{s}{(1 + s R_f C_f s)(1 + s R_t C_t)} \quad (4.2)$$

When analyzed the components that make up the transfer function can be identified. Using the rough component values as listed in table 4.1 an estimation of the values of the poles, the zero and the constant can be given. This is listed below.

- A constant of $-R_f C_t \approx -10^{-6} = -120 \text{ dB}$
- A zero at the origin
- A pole at $s = -(R_f C_f)^{-1} \approx -10^6$

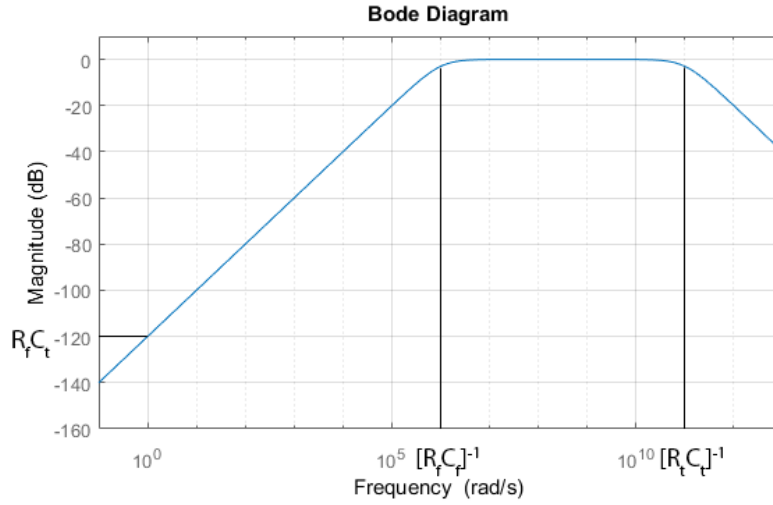


Figure 4.4: Magnitude plot of equation 4.2

- A pole at $s = -(R_t C_t)^{-1} \approx -10^{11}$

From these values a sketch of the bode plot can be made. This is shown in figure 4.4

From the magnitude plot shown in figure 4.4 it can be seen that frequencies between $-(R_f C_f)^{-1}$ and $-(R_t C_t)^{-1}$ have the largest gain. Depending on the frequency at which to measure the current through the wheel the values of components can be chosen. Furthermore, it can be seen that increasing the value of feedback resistor R_f yields practically no change in the maximum gain, but only extends the range of lower frequencies at which maximum gain is achieved. For feedback capacitor, C_f however, a smaller value does result in a higher maximum gain. This is due to the increased value at which the pole can be found. Thus in this case a lower capacitance value not only results in a higher maximum gain, it also causes the range of frequencies at which this maximum gain is achieved to shrink; the lower frequency range will have a lower gain relative to the maximum gain.

To conclude, the values chosen for the feedback resistor R_f and the feedback capacitor C_f dictate the maximum gain of the circuit and the frequencies at which this occurs, and thus should be chosen according to the desired specifications.

4.2 Frequency

This section deals with the frequency chosen at which to measure the current through the wheel. Various factors influence this choice. These factors include mechanical noise at certain frequencies due to vibrations, the frequency dependence of the permittivity of rubber, and the gain bandwidth product of practical operation amplifiers. Electromagnetic noise present in various frequency bands is not discussed here, because wires and the circuitry will be shielded. Shielding needs to be done anyway, because very small values of capacitance need to be measured.

4.2.1 Mechanical noise

One type of mechanical noise is predictable. This is the noise generated by the grooves in the tires of the car. This noise is determined by the speed at which the grooves pass i.e. driving speed of Nuna, and the radius of the wheels. The noise frequency is calculated by the amount of grooves passing by every second,

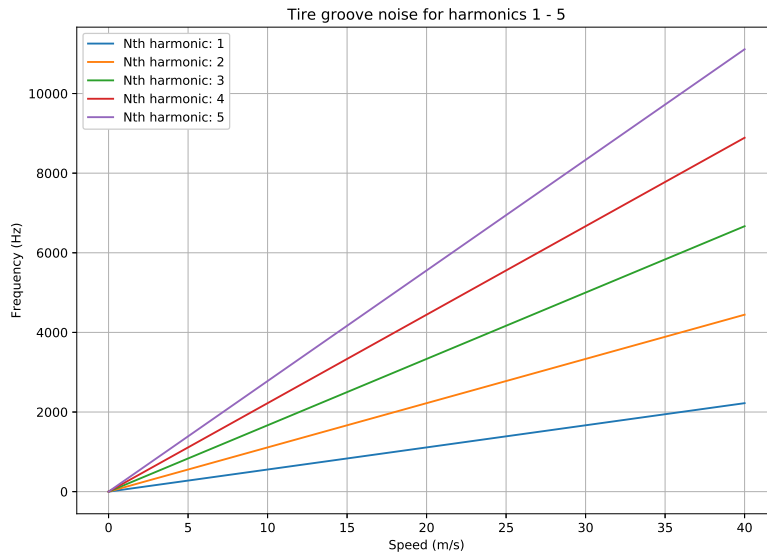


Figure 4.5: Noise frequency caused by grooves in the tires

which is the amount of grooves around the circumference of the tire times the amount of rotations per second. The code for the exact calculation can be found in appendix A and the results shown in figure 4.5. The significance of harmonics has not been tested, but it was assumed that after the 5th harmonic the noise would become insignificant.

As can be seen in figure 4.5, the frequencies containing noise barely pass the 10 kHz range. It should be noted that this is only the fifth harmonic whose noise will be negligible and only at speeds above around $36 \text{ m}\cdot\text{s}^{-1} = 36 * 3.6 = 129.6 \text{ km/hour}$, a speed that above Nuna's maximum speed. Nevertheless as a precaution a frequency above 10 kHz is chosen.

4.2.2 Permittivity

As mentioned in previous sections, the permittivity of rubber does not have a constant value for all conditions. Its permittivity is affected by the electrical signals frequency. When higher frequency components of a current pass through the rubber dielectric they undergo a lower permittivity than lower frequency components. Measurements of different types of rubber as done in "Analysis of Relative Permittivity and Tan Delta Characteristics of Silicone Rubber Based Nano-composites" [19], is shown in figure 3.2.

As can be seen from figure 3.2 rubbers permittivity is higher at lower frequencies than at higher ones. A higher permittivity, as illustrated in previous sections, is one of the most important parameters that will not only raise the difference in capacitance between different measurement levels, but will also give more resistance to any changes in permittivity in the air or due to for example dirt on the tires. While this does not set a hard limit on the possible range of frequencies, it does show us the lowest possible frequency should be chosen.

4.2.3 Gain Bandwidth Product

In previous models assumed was that the used operation amplifier had a maximum gain which was independent of frequency. In practical op amps however, this is not the case. The higher the frequency at which

the output should generate a voltage or current, the lower the maximum gain becomes. This phenomenon is described by a parameter called the Gain Bandwidth Product or GBP for short. The GBP is measured in Hz and describes the frequency at which a unity gain is expected at the output. To calculate the maximum gain at a particular frequency, equation 4.3 is used, where

- $G_{max}(f)$ is the maximum gain
- f is the frequency in Hz
- G_{GBP} is the Gain bandwidth product

$$G_{max}(f) = \frac{G_{GBP}}{f} \quad (4.3)$$

Most op amps have a GBP around 5 MHz, but if needed amplifiers with a gain bandwidth product of 20 MHz are also available. Since the charge amplifier will in an optimistic case barely surpass a gain of 10, this puts a restriction on the higher end of the possible frequency range. In this case frequencies above the MHz range. Since the subsection about permittivity concluded that the lowest possible frequency should be chosen, the GBP of the amplifier does not have to be larger than the average op amps.

In conclusion, the lowest possible frequency should be chosen to be used as the carrier wave, because this gives us the desired high permittivity of rubber. In this case keeping the restriction due to mechanical noise in mind, a frequency of 10 kHz should be chosen if feasible.

4.3 Decoding the signal

The output of the charge amplifier shown in 4.3, still outputs an alternating voltage signal. The information about the capacitance of the wheel-system is stored in the amplitude of this signal. While the waveform can be converted to the digital domain with sufficient sampling, converting the AC-signal to DC first is in this case needed. This is because processes such as centering the possible output voltage around 2.5 V and amplifying to yield a voltage range from 0 to 5 V, needed for the analog to digital converter, is easier with DC signals than with AC signals.

4.3.1 AC to DC conversion

To convert this amplitude modulated signal to a steady DC voltage, a rectifier is used. Two options to this include using a full wave rectifier and a half wave rectifier. A half wave rectifier is simpler but the outputted DC signal will also contain more ripple, which gives more deviation from the AC signals amplitude. Since small differences in voltages need to be measured, a more rectifier with less ripple would be preferred. In this case a full bridge rectifier, would be the first choice. The better ripple characteristics comes at the price of more complexity.

Figure 4.6 shows the circuit of the rectifier that will be used. Its input, V_{in} will be the AC signal, and this will be converted to a DC signal on output, V_{out} . It shows the diode bridge, formed by D1, D2, D3 and D4 that does the actually rectifying, while the capacitor smooths the DC signal. In this case a transformer is also needed. This is because galvanic isolation is needed. The need for galvanic isolation stems from the desire of a common ground between input V_{in} , and output V_{out} . The common ground is needed for next amplification stages.

The diode bridge can be formed from regular diodes with a threshold voltage well below the AC signals amplitude. The winding ratio of the transformer only needs to be 1:1 since its purpose is electrical isolation. If needed the AC voltage can also be amplified here, which would require a different winding ratio. This is determined after testing with the real charge amplifier. The value of the capacitor that smooths the DC

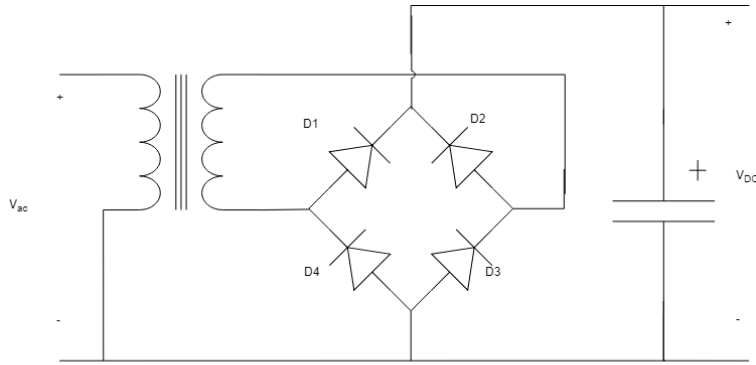


Figure 4.6: Full bridge rectifier with common ground

signal, should be large enough for the ripple to not be concern. The amount of ripple can be calculated using equation 4.4, where

- V_{pp} is the peak to peak voltage of the ripple
- I is the current though the circuit
- f is the AC frequency
- C is the capacitance of the smoothing capacitor

$$V_{pp} = \frac{I}{2fC} \quad (4.4)$$

As seen in equation 4.4, the needed capacitance depends on the current. Which needs to be depends on actual model values that will be determined during testing. So the capacitors value will also be determined after testing.

4.3.2 DC processing

The output of the rectifier circuit, illustrated in 4.6, could be in range 10 V. Since a change of capacitance due to rubber wear will be around 5% of the total capacitance, a 20 V signal will only change by about $10 * 0.05 = 0.5$ V. In this case centering the mean capacitance output voltage to 2.5 V and amplifying to increase the 0.5 V to a range of 3.3 V would be needed for the ADC. This can be achieved by another amplification stage.

The circuit of this amplification stage is shown in figure 4.7. It consists of a voltage divider, formed by resistors R1 and R2, to create a bias voltage to center the output and a amplification voltage amplifier, formed by the operational amplifier and R3 and R4. The voltage dividers output voltage, V_b is given by equation 4.5. The amplifiers output is given by equation 4.6. The values of the resistors should be chosen so that the desired output range of 0 to 3.3 V is achieved. These will be determined after testing.

$$V_b = V_{dd} \frac{R_2}{R_1 + R_2} = 12 \frac{R_2}{R_1 + R_2} \quad (4.5)$$

$$V_{out} = -V_{in} \frac{R_4}{R_3} + V_b \left(1 + \frac{R_4}{R_3}\right) \quad (4.6)$$

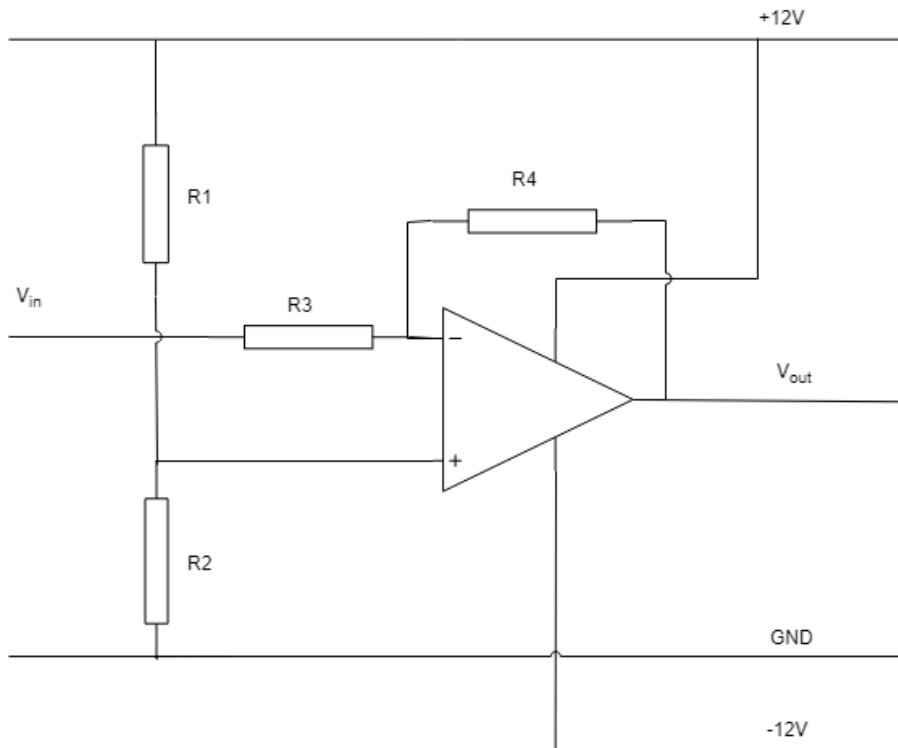


Figure 4.7: Voltage to voltage amplifier with bias voltage

Amplifier	LF356	AD745
Input offset voltage	3 mV	0.25 mV
Gain Bandwidth Product	5 MHz	20 MHz
Input noise voltage 1 kHz	$12 \text{ nV}/\sqrt{\text{Hz}}$	$3.2 \text{ nV}/\sqrt{\text{Hz}}$
Input noise current 1 kHz	$0.1 \text{ pA}/\sqrt{\text{Hz}}$	$6.9 \text{ fA}/\sqrt{\text{Hz}}$

Table 4.2: Comparison between LF356 and AD 745

4.4 Operational amplifier

For the circuit two operational amplifiers are needed. Two op amps are compared in this section, the cheap and readily available LF356 [22], and the AD745 [23], an op amp that is more suited for charge amplifiers. The extremely low input noise of the AD745 is what makes it suitable in these circuits. Since the desire for low noise is also of great importance in measuring a small value of capacitance the AD745 is also desirable in our case. Some relevant parameters of both the LF356 and the AD745 are shown in table 4.2.

4.5 Supply voltage and alternating signal

The operational amplifiers need a positive voltage, +12V and a negative voltage, -12V to operate. In the Nuna a +12V supply is readily available in the car. With the use of a voltage converter, which is able to convert this to a negative voltage, the negative -12V can be created. Various voltage converters exist, one that is able to handle voltages up to 18V is the LT1026 [24]. This converter needs two external capacitors to operate as a positive to negative converter configuration. The LT1026 with its pins and the needed configuration is shown in figure 4.8.

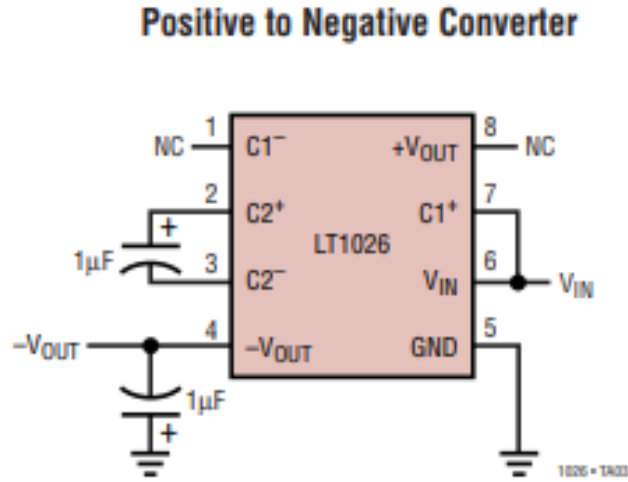


Figure 4.8: The LT1026 in the needed configuration

The alternating voltage signal will be supplied by a micro controller. This micro controller will create 5V peak to peak signal. The amplitude of this wave however, is most likely not sufficient. The needed amplitude of the signal depends on the actual gain of the charge amplifier and the amount of noise present. While the winding ratio of the transformer is to be determined, the transformer is added to the circuit. After raising the voltage of the signal using a transformer, the wave form might still contain other frequencies than the desired 10 kHz. To remove unwanted frequencies from the signal, a low pass filter is needed. The low pass filter is implemented using a resistor and a capacitor with transfer function given by equation 4.7, where

- $H(s)$ is transfer function
- R is the resistance
- C is the capacitance

$$H(s) = \frac{1}{1 + sRC} \quad (4.7)$$

With the added circuitry the entire designed circuit is shown in figure 4.9. While some component values are still undecided and some components may be added or removed, this circuit gives an overview of the final product.

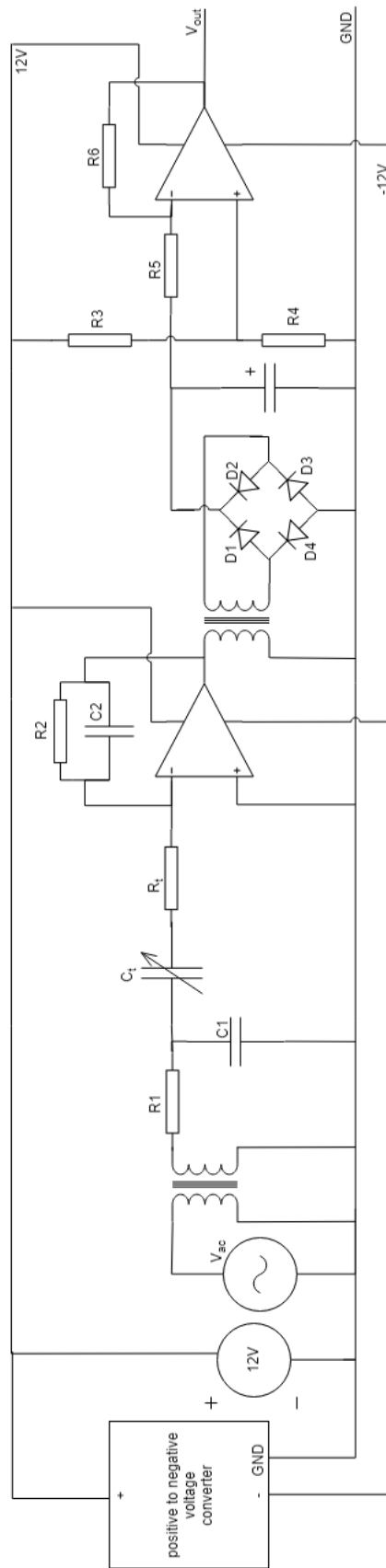


Figure 4.9: Designed circuit overview

Chapter 5

Simulations

In order to substantiate the choice of component values, a simulator was used. Noise, magnitude and phase plots were made using Python with ngspice as a simulation back-end. Python code was written to parse the results from ngspice directly to a plot. The feature was also added to sweep through multiple values of a component (R, C or L) and show the results in one plot. Spice inherently supports the feature of component sweeps, but this was done through Python to more easily save the results of each component in a separate file. The simulations assume a sinusoidal input voltage with an amplitude of 1 volt. Code can be found in appendix A.

5.1 Ngspice

Ngspice is an open-source command line based simulator. The advantage of using Ngspice over PSPICE is that it comes fully featured for free and allows the use of external models. For simulation, netlists are loaded in the simulator and run. Netlists are a text description of an electronic circuit. The netlist provides all components, component values and sources. The netlist also provides commands for the simulator such as which values to print and it even allows scripts to be used [25]. Often, SPICE models are provided for semiconductor devices such as op amps by the manufacturer, such as the LF356 which was used in the circuit discussed earlier in this chapter. All netlists used can be found in appendix B.

5.2 KiCad

KiCad is an open-source electronics schematic editor and PCB designer. A nice extra feature is the ability to export a drawn schematic to a netlist. This helps with maintaining oversight of the netlist. This program will most likely also be used when a PCB is designed, however due to time constraints this might not be possible.

5.3 Python parser

To plot results from the simulation file, a Python parser was written. Python allows shell commands to be run directly, so ngspice can be started and run from the Python script. The simulation result from ngspice is written to a text file which is parsed to arrays. These arrays contain all data required for plotting, such as voltage and frequency. Plotting and calculations were done using the numpy and matplotlib libraries.

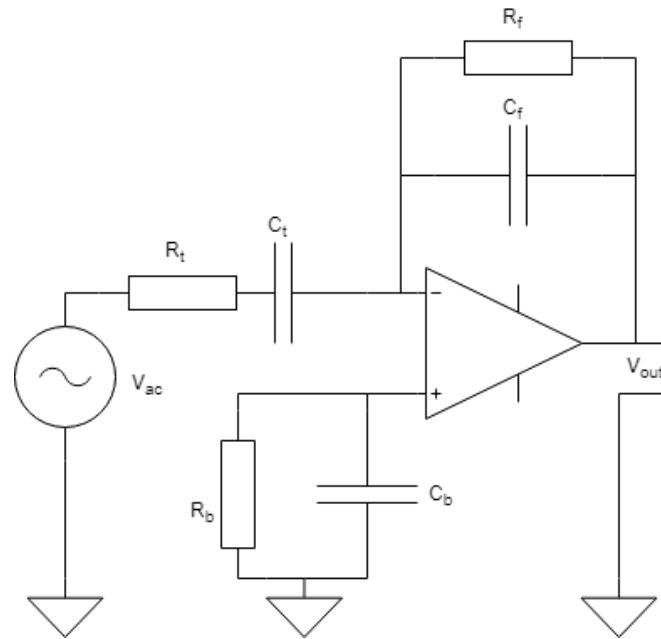


Figure 5.1: Charge amplifier circuit with added feedback resistor and bias current compensation

Component	Rough value
R_t	10Ω
C_t	various values
R_f	$7.75 \cdot 10^6\Omega$
C_f	$1 \cdot 10^{-12} \text{ F}$
Op amp	LF356

Table 5.1: Values of components

Numpy and matplotlib allow for Matlab-like operations on data, which is very convenient. Voltage arrays were converted to gain using equation 5.1.

$$\text{Gain (dB)} = 20 \log_{10} \left(\frac{V_{out}}{V_{in}} \right) \quad (5.1)$$

5.4 Gain phase simulations

First, gain phase simulations are done with the charge amplifier circuit shown in 5.1. The components used are given by table 5.1. These components were chosen because they were readily available for testing. The gain phase simulations plots are shown in figure 5.2 and some characteristics corresponding to this plot are given by table 5.2.

As can be seen from the plot, simulating with a non ideal op amp drastically reduces the upper cutoff frequency which was calculated during design. This is due to the used op amp having a gain bandwidth product of 5 MHz. As also mentioned in Design, the used frequency would ideally be 10 kHz. As seen in the plot at this frequency the transfer function doesn't have maximum gain. This is undesirable and so a bigger value for R_f is needed.

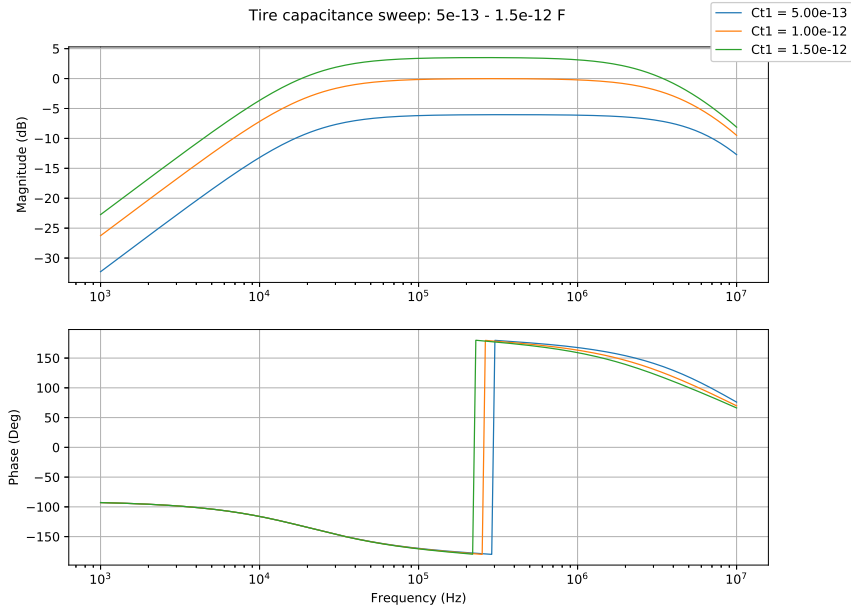


Figure 5.2: Magnitude and phase plot of tire capacitance from 0.5 pF to 1.5 pF of the circuit without compensation.

Tire capacitance	Peak gain	Lower cutoff frequency	Upper cutoff frequency	Bandwidth
0.5 pF	-6.03 dB	20.9 kHz	5.75 MHz	5.73 MHz
1 pF	-0.01 dB	20.9 kHz	3.98 MHz	3.96 MHz
1.5 pF	3.51 dB	20.9 kHz	3.02 MHz	2.51 MHz

Table 5.2: Table showing characteristics of the charge amplifier circuit with no compensation resulting from simulation in ngspice. Feedback resistor is 7.75 M Ω .

5.5 Noise simulations

Johnson-Nyquist noise or thermal noise introduced by resistive elements can be calculated by equation 5.2, which gives the one-sided noise spectral density in V^2/Hz . T being the temperature in kelvin and k_B being Boltzmann's constant. In a specific bandwidth B , the total RMS noise voltage is described by equation 5.3. The noise calculation is done over a specific bandwidth, in this case being the bandwidth of the charge amplifier. As the charge amplifier is essentially a current to voltage amplifier, the noise voltage at the output reduces for a lower noise current at the input. The feedback network of the amplifier converts the current through the tire capacitance to a voltage at the output. By applying Ohm's law, the RMS noise current can be described by equation 5.4. Hence, a higher resistor value in the feedback network will cause a reduction in output noise voltage. This was also observed in simulations when a high value feedback resistor was used.

As ngspice also offers the ability to simulate noise, this was used to calculate output noise power. The simulator replaces every resistive component with an equivalent noise source as described in the previous section, after which the noise power is referred to a source at the input of the circuit. A shell script was written to parse the output of noise simulations to a python plotting script. The code of the shell script can be found in appendix C.

$$\overline{V^2} = 4k_B T R (V^2/Hz) \quad (5.2)$$

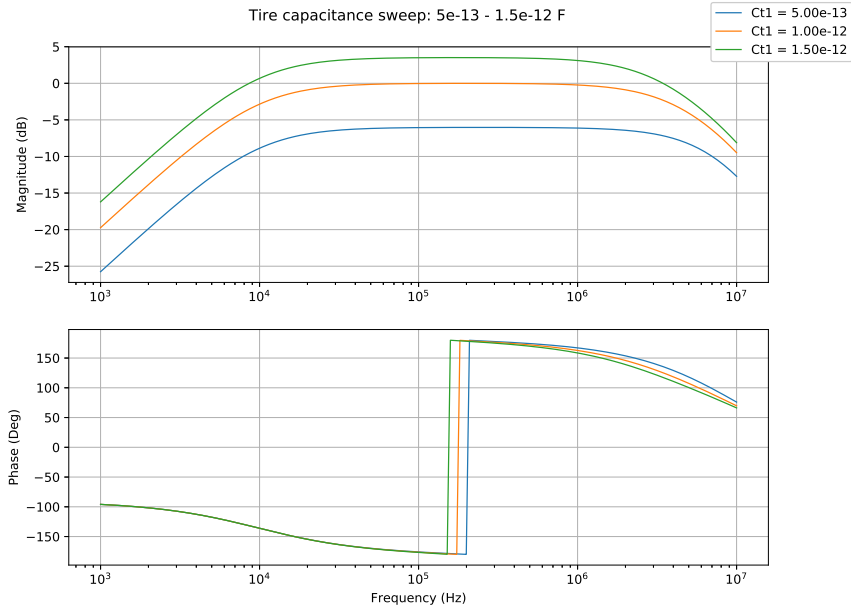


Figure 5.3: Magnitude phase plot of tire capacitance from 0.5 pF to 1.5 pF of the circuit without compensation and a 16.5 MΩ feedback resistor

Tire capacitance	Peak gain	Lower cutoff frequency	Upper cutoff frequency	Bandwidth
0.5 pF	-6.03 dB	10 kHz	5.75 MHz	5.73 MHz
1 pF	-0.01 dB	10 kHz	3.98 MHz	3.97 MHz
1.50 pF	3.51 dB	10 kHz	3.02 MHz	3.01 MHz

Table 5.3: Table showing characteristics of the charge amplifier circuit with no compensation resulting from simulation in ngspice. Feedback resistor adjusted to 16.5 MΩ.

$$V_{rms} = \sqrt{4k_B T R B} \quad (5.3)$$

$$I_{rms} = \sqrt{\frac{4k_B T B}{R}} \quad (5.4)$$

Figure 5.4 shows simulated noise power of charge amplifier circuit with no compensation using the LF356. Noise was simulated assuming a 1 pF tire capacitance. The total output noise power over a bandwidth of 3.61 MHz was found to be 3.368e-05 V², with cutoff frequencies specified in table 5.4.

Tire capacitance	Peak gain	Lower cutoff frequency	Upper cutoff frequency	Bandwidth
0.5 pF	-6.01 dB	10 kHz	1.20 MHz	1.19 MHz
1 pF	-0.01 dB	10 kHz	1.20 MHz	1.19 MHz
1.50 pF	3.53 dB	10 kHz	1.15 MHz	1.14 MHz

Table 5.4: Table showing characteristics of the charge amplifier circuit with no compensation resulting from simulation in ngspice. Feedback resistor adjusted to 16.5 MΩ and the op amp used is the AD745.

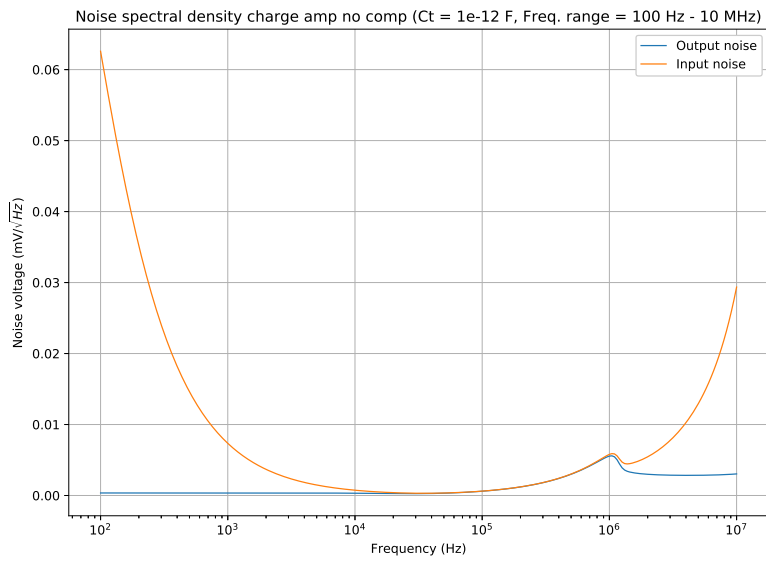


Figure 5.4: Noise simulation with LF356 and tire capacitance at 1 pF. Total output noise power over bandwidth 20.9 kHz - 3.98 MHz: $4.210e-05 V^2$

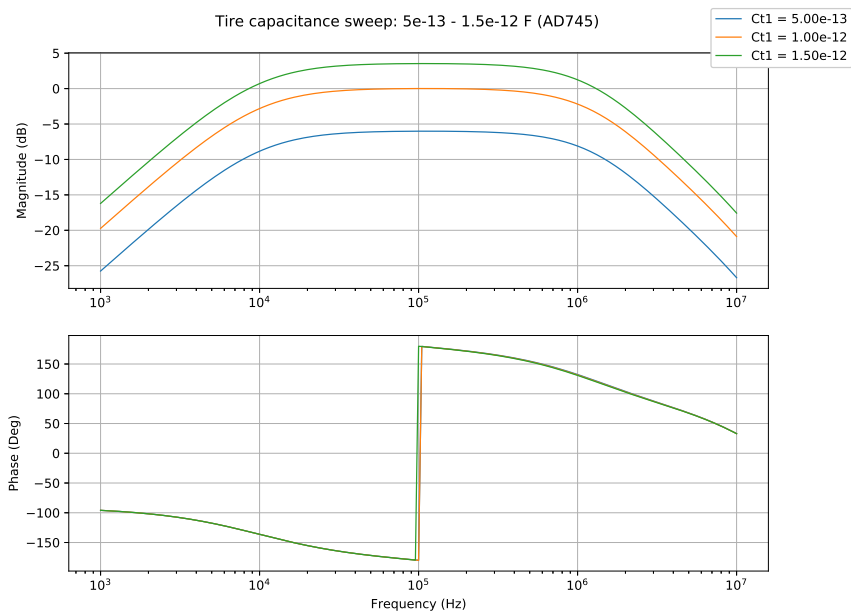


Figure 5.5: Magnitude phase plot of tire capacitance at 0.5 pF - 1.5 pF using the AD 745.

5.6 Signal to noise ratio

Power in an electrical signal is given by 5.5. Which reduces to $P = V^2$ for a normalized resistance of 1 Ω . For a sinusoidal voltage with amplitude A, the signal power averaged in time is given by the power in a period divided by the period T as shown in equation 5.6.

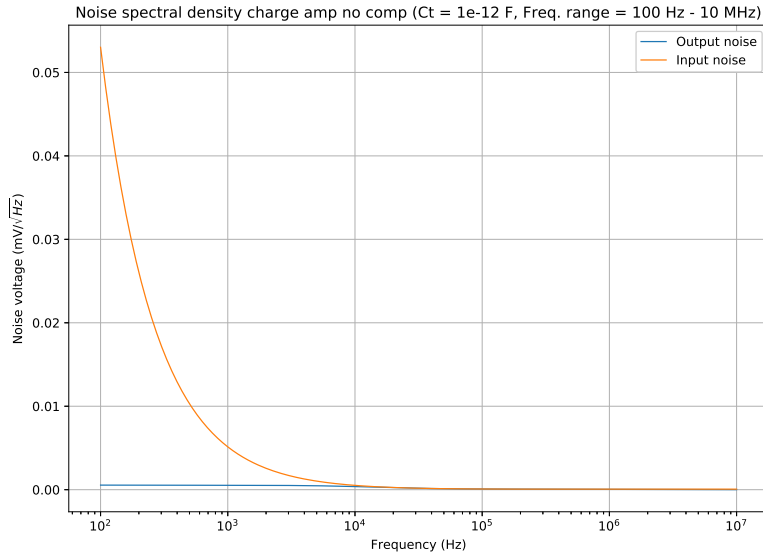


Figure 5.6: Noise simulation with AD745 and tire capacitance at 1 pF. Noise power in frequency range 10 kHz - 1.20 MHz: $5.782e-09 V^2$.

$$P = \frac{V^2}{R} \quad (5.5)$$

$$P_{avg} = \frac{1}{T} \int_{t-\frac{1}{2}T}^{t+\frac{1}{2}T} (A \sin(\omega t))^2 dt = \frac{A^2}{2} \quad (5.6)$$

The signal to noise ratio can be calculated using equation 5.7. From the simulations, only the output noise is relevant. In the simulations, the input voltage has an amplitude of 1 V, and at a gain of 0 dB the output is equal to the input. Therefore, V_{out} can be set to 1 and V_{noise} to $5.782e-09$ and $4.210e-05$ for the AD745 and LF356 respectively. The results can be seen in table 5.5. The much greater signal to noise ratio of the AD745 is probably due to the much lower input noise current.

$$20 \log_{10} \left(\frac{V_{out}}{V_{noise}} \right) = SNR \quad (5.7)$$

Operational amplifier	SNR
LF356	87.52 dB
AD745	164.76 dB

Table 5.5: Resulting signal to noise ratio for both amplifiers

5.6.1 Charge amplifier without compensation

The output noise power of the charge amplifier with compensation was also simulated. The compensation had no effect on the output noise, and the plot was almost practically the same as figure 5.4. As expected, the gain and bandwidth also remained unchanged, hence it was not used in the design.

Chapter 6

Testing

Only so much is revealed about the real circuit when simulated. Testing the circuit in the real world where background noise and non ideal components is therefore investigated. This chapter discusses the tests that were carried out to see whether the designed circuit achieves the desired requirements. Both a static and dynamic test setup were created and are both covered in this chapter.

The following equipment was used:

- Oscilloscope to compare input wave to output wave
- Function generator to form the desired wave form
- +15 V to -15 V power Supply to power the op amp

Before testing the circuitry with the actual wheel capacitance tests are done using a known capacitor and with the use of a parallel plate capacitor crafted from two pieces of wood with a layer of aluminum foil. The known capacitor is formed by six 10 pF capacitors in series and using three jumper caps to be able to easily change the total capacitance. The parallel plate capacitor is used to test the difference of measured capacitance when a different dielectric is placed in between, in this case a piece of worn rubber, a piece of new rubber and air. Figure 6.1 shows the handcrafted capacitor.



Figure 6.1: Parallel plate capacitor formed by two pieces of wood and aluminum foil

For the static test setup containing the wheel and plates a wooden board was used to mount the plates. An image of this setup is shown in figure 6.2. During first tests wires used to connect to plates to the circuitry were not shielded. This however resulted in a lot of noise at unwanted frequencies. Due to this shielded wire are used wherever possible.



Figure 6.2: Wheel plate capacitor setup

Different wheel types with different tires are provided by Nuna. The ones of interest in this case is a carbon fibre wheel with a worn tire and one with a new tire. The difference in tire wear is illustrated in figure 6.3 and figure 6.4.



Figure 6.3: Worn tire piece

For first tests only the charge amplifier circuit is made. The components used in this circuit are listed in table 6.1. These components were chosen because they were closest to the desired values to achieve the desired specifications, at the time of testing. Future testing may involve other valued components and the AD745 op amp, whose low noise better fits this specific application. An image showing the entire connected setup using the wheel capacitance is shown in figure 6.5.



Figure 6.4: Tire without wear

Component	Rough value
R_t	10Ω
C_t	various values
R_f	$7.75 \cdot 10^6\Omega$
C_f	$1 \cdot 10^{-12} \text{ F}$
Op amp	LF356

Table 6.1: Values of components

6.1 Dynamic testing

A dynamic test setup was created to test the charge amplifier circuit while the wheel is rotating. This setup uses the full circuit described in figure 6.6. For these tests the in-wheel motor of Nuna8 is used and the wheel is connected to the test vehicle used by the Nuon Solar Team. The motor resides in the rim of the wheel. This setup was created to test whether the tire wear is measurable on the same wheel, measured over a longer period, while the tire is being worn down gradually (similar as in a real race). The wearing down would be done using a file or sandpaper being pressed against the tire while rotating the wheel. The output results are logged using the internal ADC of the microcontroller listed below. The full dynamic test setup can be seen in figure 6.7. The following equipment was used during the tests:

- Fluke 117 multimeter for output voltage measurements
- Testo 880 IR camera for temperature measurements
- Tektronix TDS2024B oscilloscope
- Agilent 33521A waveform generator
- STM32F091 Nucleo64 MCU for analog-to-digital conversion

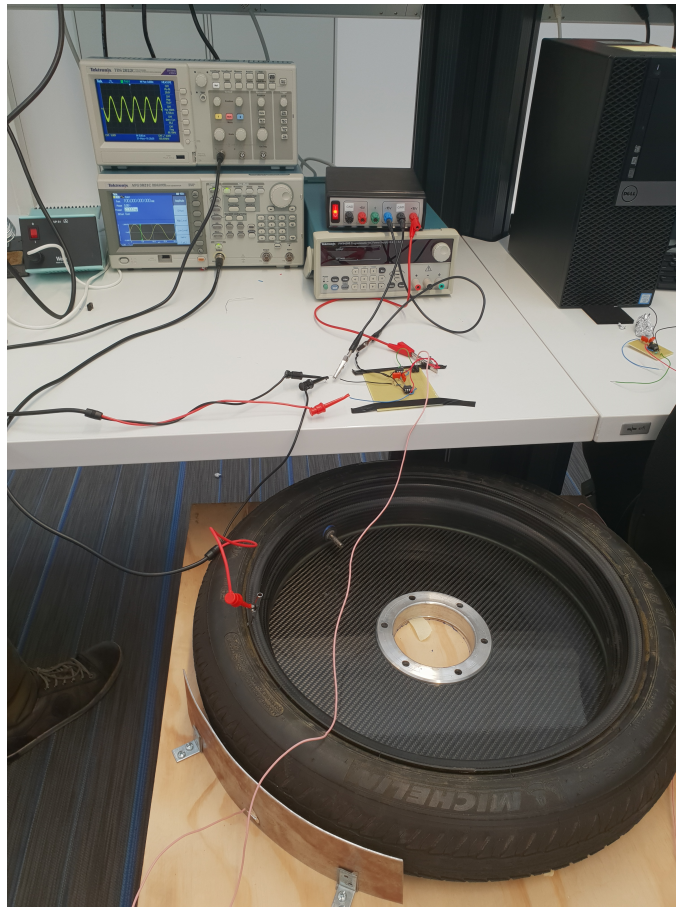


Figure 6.5: Picture showing the entire test setup to measure the wheel capacitance

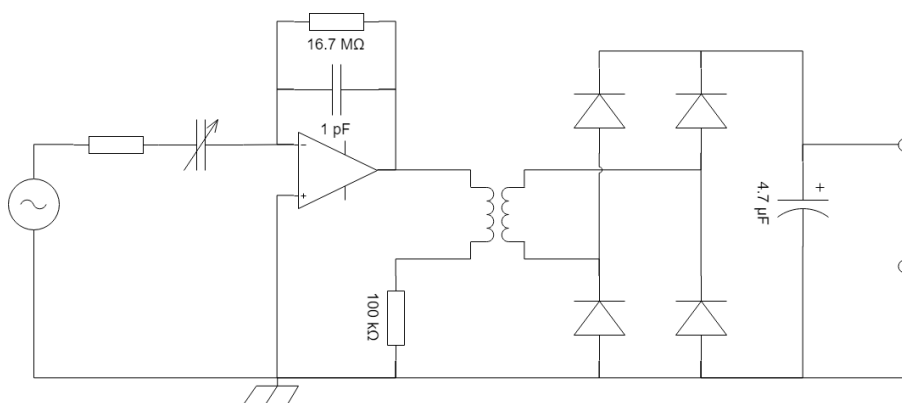


Figure 6.6: Circuit used during dynamic testing.

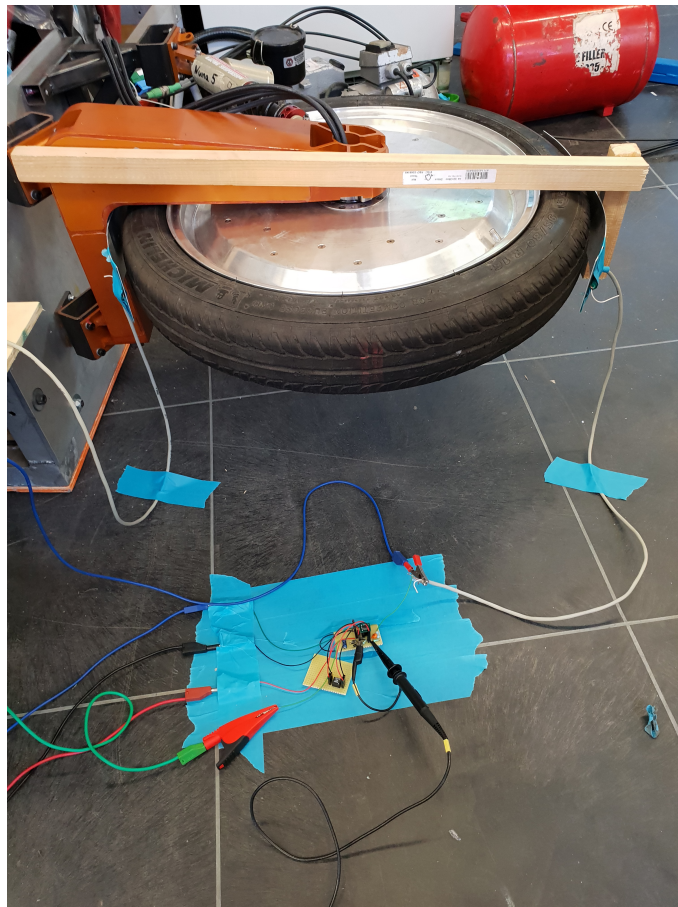


Figure 6.7: Figure showing the dynamic test setup with amplifier circuit connected.

Chapter 7

Results

The circuit shown in figure 7.1, is tested in various ways in this chapter. The components used are given by table 7.1. As seen during simulation these components do not give the desired transfer function characteristics at frequency 10 kHz. Nevertheless this circuit is tested because these components were available at the time of testing and because the reliability of the simulation can be tested.

First, the circuit is tested with the use of various known capacitors. Then, a parallel plate capacitor is formed, with which the circuit is tested with different dielectrics. Lastly, the wheel capacitor is tested. In all cases the capacitance of the capacitor in question is measured using a the RLC200 by DIGIMESS. Then then gain achieved using the capacitor is measured at different frequencies. This is done with the use of a function generator and an oscilloscope. In this case the function generator used is the TEKTRONIX AFG3021C and the oscilloscope is the TEKTRONIX TDS 2022C.

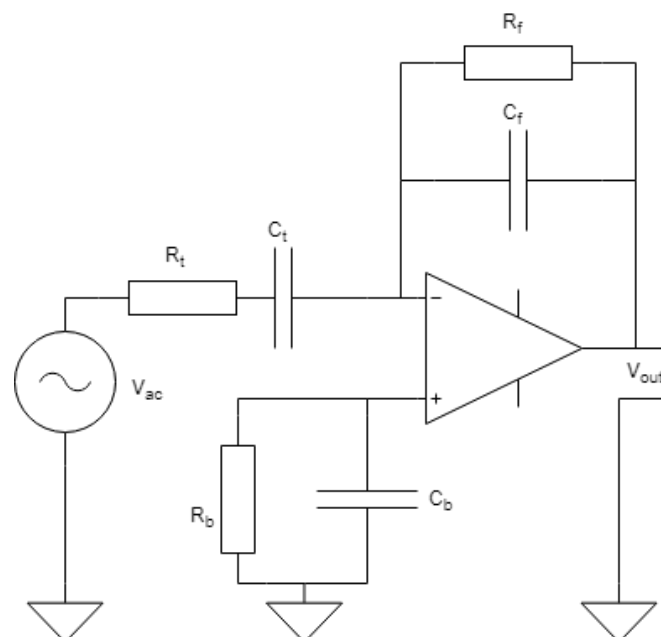


Figure 7.1: Charge amplifier circuit with added feedback resistor and bias current compensation

Component	Rough value
R_t	10Ω
C_t	various values
R_f	$7.75 \cdot 10^6\Omega$
C_f	$1 \cdot 10^{-12}$ F
Op amp	LF356

Table 7.1: Values of components

Amount of capacitors	measured capacitance
6	1.7
5	2.0
4	2.5
3	3.4

Table 7.2: Capacitance of 10 pF capacitors in series

7.1 Testing known capacitors

First six 10 pF capacitors are placed in series with jumpers used to short up to three capacitors. This gives four possible capacitor values as given by table 7.2. For this first test, three capacitors in series were used (3.4 pF). The peak to peak input and output voltages for different frequencies is shown in figure 7.3. For a 3.4 pF capacitance a maximum gain is achieved in the frequency range 50 kHz to 200 kHz. The gain here is equal to 1.8.

7.2 Testing a parallel plate capacitor

For this test a parallel plate capacitor is made using aluminum foil wrapped around pieces of wood. The dimensions of this capacitor are shown in table 7.4

f (kHz)	V_{in}	V_{out}
10	6.24	8.10
20	6.24	10.0
30	6.24	10.5
40	6.24	10.8
50	6.24	11.0
60	6.24	11.0
80	6.24	11.0
100	6.24	11.0
120	6.24	11.0
140	6.24	11.0
200	6.24	11.0
250	6.24	10.8
300	6.24	10.8
400	6.24	10.4
500	6.24	9.40

Table 7.3: 3.4 pF capacitor

Plate to plate distance	7.3 mm
Length	119.5 mm
Width	81.0 mm

Table 7.4: Dimensions of the parallel plate capacitor

f (kHz)	V_{in}	V_{out}
10	2.2	12.4
20	2.2	15.8
30	2.2	16.6
40	2.2	17
50	2.2	17
60	2.2	17
80	2.2	17
100	2.2	17
120	2.2	17
140	2.2	16.8
200	2.2	15.8
250	2.2	14.8
300	2.2	12.7
400	2.2	10.8
500	2.2	6.1

Table 7.5: Parallel plate with air between

7.2.1 Air gap between plates

Putting no rubber between the plates and leaving an air gap yields a capacitance measured by the RLC200 yields a value of 21.7 pF. Then using the oscilloscope and the function generator the peak to peak input and output voltages for different frequencies is measured. The results are shown in figure 7.5. For the parallel plate capacitor with an air gap a maximum gain is achieved in the frequency range 40 kHz to 120 kHz. The gain here is equal to 7.727.

7.2.2 A layer of new rubber between plates

When the air gap between the plates is filled by a piece of new rubber tire, a capacitance of 47.0 pF is measured by the RLC200. Then using the oscilloscope and the function generator the peak to peak input and output voltages for different frequencies is measured. The results are shown in figure 7.6. For parallel plate capacitor with a piece of new rubber tire a maximum gain is achieved at a frequency of 40 kHz. The gain here is equal to 16.

7.2.3 A layer of worn rubber between plates

When the dielectric between the plates is replaced by a piece of worn rubber tire, a capacitance of 31.2 pF is measured by the RLC200. Then using the oscilloscope and the function generator the peak to peak input and output voltages for different frequencies is measured. The results are shown in figure 7.9.

For parallel plate capacitor with a piece of new rubber tire a maximum gain is achieved at a frequency of 40 kHz. The gain here is equal to 15.6.

f (kHz)	V_{in}	V_{out}
10	1.3	16.4
20	1.3	20
30	1.3	20.4
40	1.3	20.8
50	1.3	20.6
60	1.3	20.4
80	1.3	20
100	1.3	19.4
120	1.3	18.6
140	1.3	18.2
200	1.3	16.2
250	1.3	14.6
300	1.3	13.2
400	1.3	10.8
500	1.3	9.2

Table 7.6: Parallel with new rubber tire between

f (kHz)	V_{in}	V_{out}
10	1.1	12.8
20	1.1	16.0
30	1.1	16.8
40	1.1	17.2
50	1.1	17.0
60	1.1	16.8
80	1.1	16.4
100	1.1	16.2
120	1.1	15.6
140	1.1	15.0
200	1.1	13.6
250	1.1	12.2
300	1.1	11
400	1.1	9.2
500	1.1	7.8

Table 7.7: Parallel with worn rubber between

7.3 Testing wheel tire

Testing the with the capacitor formed by placing plates across the wheel is the test that matters the most. In this section two cases are tested. The first is the case when a wheel with a new tire is measured. The second is with a wheel with a worn tire is tested. In both cases no accurate reading could be given by the RLC200, this is most likely due to the limited accuracy of the RLC200.

7.3.1 Wheel with new tire between plates

For the plate capacitor with a wheel with new tires a maximum gain is achieved at a frequency of 10 kHz. The gain here is equal to 0.87.

f (kHz)	V_{in}	V_{out}
10	21.0	18.2
20	21.0	17.2
30	21.0	16.3
40	21.0	15.6
50	21.0	15.2
60	21.0	14.8
80	21.0	14.2
100	21.0	13.9
120	21.0	13.6
140	21.0	13.4
200	21.0	12.8
250	21.0	12.3
300	21.0	11.8
400	21.0	11.0
500	21.0	10.0

Table 7.8: Plates with new tire piece

f (kHz)	V_{in}	V_{out}
10	21.0	13.9
20	21.0	14.2
30	21.0	13.9
40	21.0	13.7
50	21.0	13.3
60	21.0	13.1
80	21.0	12.9
100	21.0	12.7
120	21.0	12.5
140	21.0	12.3
200	21.0	11.8
250	21.0	11.4
300	21.0	11.0
400	21.0	10.2
500	21.0	9.70

Table 7.9: Plates with worn tire piece

7.3.2 Wheel with worn tire between plates

For the plate capacitor with a wheel with worn tires a maximum gain is achieved at a frequency of 20 kHz. The gain here is equal to 0.67. A plot of the data of the parallel plate capacitor with air, a worn tire piece and a new tire piece can be seen in figure 7.2.

7.4 Dynamic testing

During dynamic testing, it was observed that the output of the amplifier circuit fully saturated to 12 V. Further inspection of the signals showed the signal which drives the motor caused a huge amount of noise at 10 kHz and harmonics. The noise signal propagated through the metal rim of the wheel and picked up by the capacitor plates, which function as antennas for the signal. Also, while the motor was off there was noise present from other sources. This noise could be reduced when the back side of the capacitor plates were shielded, further confirming the plates function as antennas for noise.

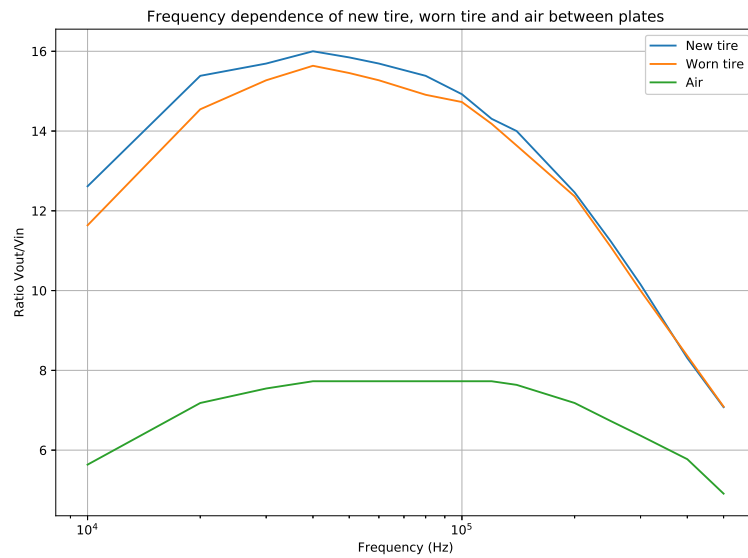


Figure 7.2: Plot showing the gain over a frequency range for air, a worn tire and a new tire between the parallel plate capacitor.

Another problem which was found while testing the test vehicle the wheel is connected to. This is a almost fully metal structure, which was also observed to cause a significant amount of noise during testing. An attempt to ground the test vehicle was made, which reduced the output noise slightly. The aforementioned problems resulted in the inability to test whether tire wear was measurable on the same tire while being worn down gradually. However, using the dynamic setup an observable difference in output voltage of around 20 mV was measured by wearing down a small part of the tire while leaving the motor off. This was essentially like doing a static test on the dynamic test setup.

Chapter 8

Conclusion

As can be seen from the results of the measurements in static tests, on average the frequency at which maximum gain is achieved is lower for measurements that used rubber as a dielectric. This is expected due to the higher relative permittivity at lower frequencies.

Comparing the results of a worn tire and new one at the desired frequency of 10 kHz yields a the largest voltage difference of 4.3 V. This is also expected because higher permittivity is the most important factor for measurable difference. At this frequency the percentage difference is 23.6%. This percentage is well above the calculated 4.7% and this raises the question why this difference is so huge. While the ignored fringing effects and perhaps a higher permittivity of the tires than expected may raise the calculated voltage a bit, this alone can not account for the measured results. Another possibility is that the change of capacitance of the tire changes the transfer function of the entire circuit in such a way that the lower cutoff frequency is changed to a higher value causing a non maximum gain. This reasoning is supported by the results from the measurements with a worn tire, where the maximum gain is not achieved at 10 kHz like that new tire, but at 20 kHz. Yet another plausible explanation is small differences in the different wheels or in the tires. This may be due to manufacturing inaccuracies.

An attempt was made to do a dynamic test, wearing down a tire gradually while rotating and logging the resulting output voltage of the circuit using the ADC. Due to the large amount of noise caused by the motor, this test could not be performed successfully. The motor noise frequencies were at 10 kHz and harmonics, which is exactly the signal which was initially chosen as input signal. However, a static test on the dynamic test setup did show a stable difference of 20 mV at the output, which shows that the measurement principle works when no motor noise is present. Additionally, it was observed that shielding of the capacitor plates makes a significant difference in output voltage, greatly reducing noise.

8.1 Recommendations

In case of further investigation into this method of tire wear sensing, it is recommended that the motor noise frequencies are avoided and heavily filtered. In the case of the Nuna8 motor, this would entail avoiding 10 kHz and harmonics. Therefore, a signal of 15 kHz is recommended using a as narrow as possible band pass filter on 15 kHz to reduce motor noise. It should be noted that this frequency might be different when using a different motor.

The system also greatly benefits from shielding the capacitor plates. Therefore it is recommended that further tests are done using carbon fibre wheel hoods to cover the tires and grounding them to the body of the car. It is conjectured that this will provide shielding for the capacitor plates and significantly reduces noise.

The last recommendation is that further investigation on the effect of temperature and sand/dirt on tire permittivity should be done. As mentioned in chapter 4 this may play a large role in the capacitance measurement and may need to be compensated for.

If these recommendations are implemented, it is believed that capacitively sensing rubber thickness is possible, since the results from static testing are promising. The system is quite delicate and sensitive to noise, therefore it might not be up to par with the robustness standards of the Nuon Solar Team. In the end it is up to the team to determine whether more development into this method is granted.

Appendices

Appendix A

Python code

A.1 Current sensor plots

A.1.1 Linearity

```
1 import matplotlib.pyplot as plt
2 import numpy as np
3 import re
4
5 # Temperature offset measurements
6 current = []
7 temperature = []
8 vout = []
9 voltage_drop = []
10
11 measurements = []
12 with open('hall_measurements.txt') as file:
13     next(file)
14     for line in file:
15         measurements.append(tuple([float(i) for i in re.findall(r'[\w
16             ↪ \.-]+', line)]))
17
18 measurements = sorted(measurements, key=lambda x: x[0])
19
20 for measurement in measurements:
21     current.append(float(measurement[0]))
22     temperature.append(float(measurement[1]))
23     vout.append(float(measurement[2]))
24     voltage_drop.append(float(measurement[3]))
25
26 vout = np.array(vout)[np.greater_equal(np.array(current), 0)][:-1]
27 current = np.array(current)[np.greater_equal(np.array(current), 0)
28     ↪ ][:-1]
29 # Least squares to compute line fit
30
```

```

31 A = np.vstack([current, np.ones(len(current))]).T
32 a, b = np.linalg.lstsq(A, vout)[0]
33
34 true_line = a*current+b
35 error = np.abs(np.subtract((a*current+b), vout))
36 mean_error = np.mean(error)
37 print(mean_error)
38 # fig = plt.figure(figsize=(10,7))
39 # ax = fig.add_subplot(111)
40 # ax.set_xlabel('Current (A)')
41 # ax.set_ylabel('Absolute error (mV)')
42 #
43 # line2d = ax.plot(current, np.abs(np.subtract((a*current+b), vout)),
44 #                 ↪ label='Error')
45 # #line2d = ax.plot(current, a*current+b, label='True line')
46 # #ax.plot(current, vout, 'o', label='Measurements')
47 #
48 # ax.plot([np.amin(current), np.amax(current)], [mean_error,
49 #                 ↪ mean_error], label='Mean', color='r', linestyle='--', linewidth
50 #                 ↪ =1)
51 #
52 # plt.title('Absolute error of measured voltage compared to fitted
53 #           ↪ line')
54 # fig.savefig('hall_sens_linearity.eps', dpi=600, format='eps')
55 # fig.tight_layout()
56 # plt.legend()
57 # plt.grid(True)
58 # plt.show()
59
60 # First subplot
61 fig = plt.figure(figsize=(8, 10))
62 ax = fig.add_subplot(211)
63 ax.set_xlabel('Current (A)')
64 ax.set_ylabel('Output voltage (mV)')
65 ax.plot(current, vout, 'o', label='Output voltage measurements', ms=5)
66 ax.plot(current, a*current+b, label='Fitted line', linestyle='-', color
67         ↪ ='r', linewidth=0.75)
68 plt.title('Output voltage linearity')
69 plt.legend()
70 ax.grid(True)
71 plt.legend()
72
73 # Second subplot
74 ax2 = fig.add_subplot(212)
75 ax2.plot(current, error, label='Absolute error')
76 ax2.plot([np.amin(current), np.amax(current)], [mean_error, mean_error
77         ↪ ], label='Mean', color='r', linestyle=':', linewidth=1)
78 ax2.set_xlabel('Current (A)')
79 ax2.set_ylabel('Absolute error (mV)')
80 ax2.grid(True)
81 plt.legend()
82 fig.savefig('hall_sens_linearity.eps', dpi=600, format='eps')
83 plt.show()

```

A.1.2 Output voltage

```

1 import matplotlib.pyplot as plt
2 import numpy as np
3 import re
4
5 # Temperature offset measurements
6 current = []
7 temperature = []
8 vout = []
9 voltage_drop = []
10
11 with open('hall_measurements.txt') as file:
12     next(file)
13     for line in file:
14         measurements = re.findall(r'[\w\.-]+', line)
15         current.append(float(measurements[0]))
16         temperature.append(float(measurements[1]))
17         vout.append(float(measurements[2]))
18         voltage_drop.append(float(measurements[3]))
19
20
21 current = np.array(current)
22 vout = np.array(vout)
23
24
25 stepsize = vout[current > 0]/current[current > 0]
26 print(np.mean(stepsize))
27
28 fig = plt.figure(figsize=(10,7))
29 ax = fig.add_subplot(111)
30 ax.set_xlabel('Current (A)')
31 ax.set_ylabel('Output voltage (mV)')
32 lns1, = ax.plot(current, vout, label='Output voltage')
33
34 ax2 = ax.twinx()
35 ax2.set_ylabel('Temperature ($^\circ$C)')
36 current_trimmed = np.array(current)[np.array(current) > 0]
37 temperature_trimmed = np.array(temperature)[np.array(current) > 0]
38
39 lns2, = ax2.plot(current_trimmed, temperature_trimmed, label='
    ↳ Temperature', color='orange')
40 handles, labels = ax.get_legend_handles_labels()
41 handles1, labels1 = ax2.get_legend_handles_labels()
42 fig.legend(handles=[handles[0], handles1[0]], labels=['Output voltage',
    ↳ 'Temperature'], loc='upper left')
43 plt.title('Measured voltage at output and temperature vs. current (
    ↳ ambient temperature = 22 $^\circ$C)')
44 ax.grid(True)
45 fig.savefig('hall_sens_voltage_temp.eps', dpi=600, format='eps')

```

```
46 plt.show()
```

A.1.3 Temperature

```

1 import matplotlib.pyplot as plt
2 import numpy as np
3 import re
4
5 # Temperature offset measurements
6
7 temperature = []
8 voffset = []
9 measurements = []
10
11 with open('hall_temp.txt') as file:
12     for line in file:
13         measurements.append(re.findall(r'[\w\.-]+', line))
14
15 for pair in measurements:
16     temperature.append(float(pair[0]))
17     voffset.append(float(pair[1]))
18
19
20 temperature = np.array(temperature)
21 voffset = np.array(voffset)
22
23 A = np.vstack([temperature, np.ones(len(temperature))]).T
24 a_temp, b_temp = np.linalg.lstsq(A, voffset)[0]
25
26 true_line_temp = a_temp * temperature + b_temp
27 error = np.abs(np.subtract((a_temp * temperature + b_temp), voffset))
28 mean_error = np.mean(error)
29 print(np.mean(true_line_temp)/true_line_temp.size)
30 print(mean_error)
31
32 # First subplot
33 fig = plt.figure(figsize=(8, 10))
34 ax = fig.add_subplot(211)
35 ax.set_xlabel('Temperature ($^\circ\text{C}$)')
36 ax.set_ylabel('Offset (mV)')
37 line2d = ax.plot(temperature, voffset, label='Offset')
38 ax.plot(temperature, true_line_temp, label='Fitted line', linestyle='--'
39     ↪ , color='r', linewidth=1)
40 plt.grid(True)
41 plt.title('Offset voltage vs. temperature (ambient temperature = 21.9
42     ↪ $^\circ\text{C}$)')
43 plt.legend()
44
45 # Second subplot
46 ax2 = fig.add_subplot(212)
47 ax2.plot(temperature, error, label='Absolute error')
```

```

46 ax2.plot([np.amin(temperature), np.amax(temperature)], [mean_error,
    ↪ mean_error], label='Mean', color='r', linestyle='--', linewidth
    ↪ =1)
47 ax2.set_xlabel('Temperature ( $\circ$ C)')
48 ax2.set_ylabel('Absolute error (mV)')
49 ax2.grid(True)
50 plt.legend()
51 fig.savefig('hall_sens_temp_offset.eps', dpi=600, format='eps')
52 plt.show()

```

A.2 Simulation code

A.2.1 Ac sweeper main

```

1 from ac_sweep_parser import *
2
3 # Helper functions
4
5
6 # Sweeper params
7
8 netlist = 'c_amp_2_no_comp_ac_AD745.cir'
9 component_name = 'Ct1'
10 start_value = 0.5e-12
11 end_value = 1.5e-12
12 n_steps = 3
13 component_values = np.linspace(start_value, end_value, n_steps)
14
15
16 # Set size and title
17
18 fig = plt.figure(figsize=(10,7))
19 component_dict = {'C': 'F', 'R': '$\Omega$', 'L': 'H'}
20 # fig.suptitle("{0} sweep {1}: {2:.2e} {3} - {4:.2e} {3}".format(
21 # netlist, component_name, start_value, component_dict[
    ↪ component_name[0]], end_value))
22
23 # Manual figure title for final plots
24 fig.suptitle("Tire capacitance sweep: {} - {} F (AD745)".format(
    ↪ start_value, end_value))
25
26 # Set magnitude axis
27
28 ax_mag = fig.add_subplot(2,1,1)
29 ax_mag.set_ylabel('Magnitude (dB)')
30 ax_mag.grid(b=True)
31
32 # Set phase axis
33
34 ax_phase = fig.add_subplot(2,1,2)
35 ax_phase.set_ylabel('Phase (Deg)')

```

```

36 ax_phase.set_xlabel('Frequency (Hz)')
37 ax_phase.grid(b=True)
38
39
40 max_y_old = float('-inf')
41 min_y_old = float('inf')
42
43 # Listing containing max gain points of components values
44 maxima_list = []
45
46 # Results to write to file
47 results_tofile = []
48
49 for i, result_file in enumerate(sweep(netlist, component_name,
    ↪ component_values)):
50     # Voltage and frequency arrays
51     v_array, f_array = get_voltage_and_freq(result_file)
52
53     # Gain and phase arrays
54     gain_array = get_gain_array(v_array)
55     phase_array = get_phase_array(v_array)
56
57     # Find band of relatively flat gain
58
59     gain_within_range = gain_array[(np.abs(np.amax(gain_array) -
    ↪ gain_array)) < 3]
60     freq_within_range = f_array[(np.abs(np.amax(gain_array) -
    ↪ gain_array)) < 3]
61     cutoff_freqs = (freq_within_range[0], freq_within_range[-1])
62     bandwidth = cutoff_freqs[1] - cutoff_freqs[0]
63
64
65     # Maximum gain points
66     max_x, max_y = get_max_gain(gain_array, f_array)
67     maxima_list.append([component_values[i], max_x, max_y])
68
69     print('{} {} max gain: {} dB at {:.2f} Hz'.format(component_name,
    ↪ result_file[-12:][:8], max_y, max_x))
70     print('Cutoff_freqs: ' + str(cutoff_freqs))
71     print('Bandwidth: ' + str(bandwidth))
72     results_tofile.append(['{} {} max gain: {} dB at {:.2f} Hz'.format
    ↪ (component_name, result_file[-12:][:8], max_y, max_x),
73                             'Cutoff_freqs: ' + str(cutoff_freqs),
    ↪ 'Bandwidth: ' + str(bandwidth)])
74
75     if max_y_old < max_y:
76         max_y_old = max_y
77         complete_max_x = max_x
78     if min_y_old > max_y:
79         min_y_old = max_y
80         complete_min_x = max_x
81
82     # Start plotting

```

```

83     ax_mag.semilogx(f_array , gain_array , label=component_name + ' = '
84         ↪ + result_file[-12:][:8], linewidth=1, antialiased=True)
85     ax_phase.semilogx(f_array , phase_array , linewidth=1, antialiased=
86         ↪ True)
87 handles , labels = ax_mag.get_legend_handles_labels()
88 plt.figlegend(handles , labels , 'upper right')
89 fig.subplots_adjust(top=0.92, bottom=0.1)
90 #fig.savefig('/home/koen/Documents/Simulation_results/Ac_sweep/{
91     ↪ _sweep-{}-{:2e}-{:2e}.eps'.format(component_name , netlist
92     ↪ [:-4],start_value , end_value) , dpi=600, format='eps')
91 file_path = '/home/koen/Documents/Simulation_results/Ac_sweep/'
92 file_name = 'final-{}_sweep-{}-{:2e}-{:2e}.eps'.format(
93     ↪ component_name , netlist[:-4],start_value , end_value)
93 fig.savefig(file_path + file_name , dpi=600, format='eps')
94 fig.show()
95
96 # Write additional info to file
97
98 with open(file_path + file_name[:-4] + '.txt', 'a') as file:
99     file.write('——' * 20 + '\n\n')
100    file.write(netlist + '\n\n')
101    file.write('——' * 20 + '\n\n')
102    for list in results_tofile:
103        for line in list:
104            file.write(line + '\n')
105            file.write('\n')
106    file.write('\n\n')
107    #for value in component_values:
108        #max_calculated_gain = 20*np.log10(7.75e6 * value) + 20*np.
109            ↪ log10(1 / (7.75e6 * 1e-12))
109        #file.write('Max calculated gain: ' + str(max_calculated_gain)
110            ↪ + '\n\n')
110    file.write('——'*20 + '\n\n')
111
112
113 # Code for calculating differences between maximum gain points
114
115 # maxima_list = np.flipud(np.array(maxima_list))
116 # for i , max_diff in enumerate(np.ediff1d(maxima_list[:,2])):
117 #     print('Gain difference between {0:.2e} and {1:.2e}: {2}'.format(
118     ↪ maxima_list[:,0][i] , maxima_list[:,0][i+1] , abs(max_diff)))
118 #print('Gain diff: {} (dB)'.format(abs(max_y_old-min_y_old)))

```

A.2.2 Ac sweeper

```

1 # This code should be able to sweep components by name
2 # Given the component name, start value, end value and amount of steps
3 # The script should be able to look in a netlist, and replace the
4     ↪ component values
4 # For now, stick to RLC components only

```

```

5
6 import numpy as np
7 import re
8 import subprocess as sp
9 import os
10 import datetime
11
12
13 def sweep(netlist, component_name, value_list):
14     # Check make directory for simulation results
15     now = datetime.datetime.now().strftime('%Y-%m-%d_%H:%M:%S')
16     directory = '/home/koen/Documents/Elektro/ngspice/
17     ↪ sim sweep_results-{}-{}'.format(netlist[: -4], now)
18     if not os.path.exists(directory):
19         os.makedirs(directory)
20
21     for component_value in value_list:
22
23         # avoid editing subcircuits by only changing the first
24         ↪ occurrence
25         first_occurrence_check = False
26
27         with open(netlist) as netlist_old:
28
29             netlist_copy_name = netlist.replace('.cir', '_copy.cir')
30             with open(netlist_copy_name, 'w') as netlist_copy:
31                 for current_line in netlist_old:
32                     # Search lines of netlist for the component
33                     find_comp = re.search(r'^{}\s'.format(str(
34                         ↪ component_name)), current_line)
35
36                     #find_comp = re.search(r'\.param\s{}'.format(
37                         ↪ str(component_name)), current_line)
38                     if find_comp and not first_occurrence_check:
39                         # Component found, replace old component
40                         ↪ value by new value and write to file
41                         new_component = re.sub(r'([\w\ -+\.\.])\W+${}
42                         ↪ , {:.2e}'.format(component_value),
43                         ↪ current_line)
44                         #new_component = re.sub(r'^\s]+$ ', '{:.2e
45                         ↪ }'.format(component_value),
46                         ↪ current_line)
47                     print(new_component)
48                     netlist_copy.write(new_component+'\n')
49                     first_occurrence_check = True
50                 else:
51                     # Component not found, copy line from old
52                     ↪ to new file
53                     netlist_copy.write(current_line)
54
55     # For every component value, create a new file to write
56     ↪ results
57     result_file_name = '{}/simresults-{}-{}-{:3.2e}.txt'.format(
58     ↪ directory, netlist[: -4], component_name, component_value

```

```

    ↪ )
47
48     with open(result_file_name, 'w') as file:
49         # Start ngspice in a shell using subprocess, write the
50         ↪ results to file
51         start_command = ["ngspice", "-b", netlist_copy_name]
52         sp.run(start_command, stdout=file)
53
54         # Generator statement for easy transfer of filename to plotter
55         yield result_file_name
56
57 if __name__ == "__main__":
58     netlist = 'amp_test.cir'
59     component_name = 'C1'
60     start_value = 10e-14
61     end_value = 10e-12
62     n_steps = 10
63
64     input_list = np.linspace(start_value, end_value, n_steps)
65
66     sweep(netlist, component_name, input_list)

```

A.2.3 Ac sweep parser

```

1 import numpy as np
2 import re
3 import matplotlib.pyplot as plt
4 from ac_sweeper import sweep
5
6 def countlines(result_file):
7     with open(result_file) as file:
8         current_line = file.readline()
9         while True:
10            try:
11                find_count = re.search('No. of Data Rows : (\d+)',
12                ↪ current_line)
13                if find_count:
14                    return int(find_count.group(1))
15                current_line = next(file)
16            except StopIteration:
17                return None
18
19 def get_voltage_and_freq(result_file):
20     n = countlines(result_file)
21     voltage = [None] * n
22     freq = [None] * n
23
24     with open(result_file) as file:
25         line_num = 0
26

```

```

27     # Extract results form result file
28     for line in file:
29         if (re.search('(-?\d+\.\d{1,6}e[+-]\d{2})', line)):
30             split_result = re.findall('(-?\d+\.\d{1,6}e[+-]\d{2})',
31                                     ↪ , line)
32             freq[line_num] = float(split_result[0])
33             voltage[line_num] = complex(float(split_result[1]),
34                                         ↪ float(split_result[2]))
35             line_num += 1
36
37     # Create numpy arrays
38     return np.array(voltage), np.array(freq)
39
40 def get_gain_array(voltage_array):
41     # compute gain and maximum
42     # gain = 20log(|Vout/Vin|) (Vin = 1 in this case)
43     return 20*np.log10(np.absolute(voltage_array))
44
45 def get_max_gain(gain_array, freq_array):
46     # get (x,y) coordinates of max gain
47     max_index = np.argmax(gain_array)
48     return freq_array[max_index], gain_array[max_index]
49
50 def get_phase_array(voltage_array):
51     # compute phase array
52     return np.angle(voltage_array, deg=True)

```

A.2.4 Noise main

```

1 import subprocess as sp
2 import matplotlib.pyplot as plt
3 import numpy as np
4 import scipy.integrate as int
5
6 script_path = '/home/koen/Documents/Elektro/Scripts/noise_parse.sh'
7 noise_netlist = 'c_amp_2_noise_no_comp_ad745.cir'
8 result_file = 'noise_sim_out.raw'
9 working_dir = '/home/koen/Documents/Simulation_results/Noise'
10 sim_range = '100 Hz - 10 MHz'
11 cutoffs = (10000.0, 1202264.0)
12 capacitance = 1e-12
13
14 def run_sim():
15     start_command = [script_path, noise_netlist, result_file,
16                     ↪ working_dir]
17     sp.run(start_command)
18 freq = []

```

```

19 o_vnoise = []
20 i_vnoise = []
21
22 run_sim()
23
24 with open('{} .txt'.format(result_file[:-4])) as result_file:
25     for line in result_file:
26         split_line = line.split(' ')
27         freq.append(float(split_line[0]))
28         o_vnoise.append(float(split_line[1]))
29         i_vnoise.append(float(split_line[2]))
30
31 freq = np.array(freq)
32 o_vnoise = np.array(o_vnoise)
33 i_vnoise = np.array(i_vnoise)
34
35 # Plotting
36 fig = plt.figure(figsize=(10,7))
37 plt.semilogx(freq, o_vnoise*1000, label='Output noise', linewidth=1,
38             ↪ antialiased=True)
39 plt.semilogx(freq, i_vnoise*1000, label='Input noise', linewidth=1,
40             ↪ antialiased=True)
41 plt.xlabel('Frequency (Hz)')
42 plt.ylabel('Noise voltage (mV/$\sqrt{\text{Hz}}$)')
43 plt.title('Noise spectral density charge amp no comp (Ct = {} F, Freq.
44             ↪ range = {})'.format(capacitance, sim_range))
45 plt.grid(True)
46 plt.legend()
47 fig.savefig('/home/koen/Documents/Simulation_results/Noise/Plots/{}_
48             ↪ {:.2e}-{:.2e}_AD745_noise_plot.eps'.format(noise_netlist[:-4],
49             ↪ cutoffs[0], cutoffs[1]), dpi=600, format='eps')
50 plt.show()
51
52 freq_range = np.logical_and(freq > cutoffs[0], freq < cutoffs[1])
53
54 # Total noise power calculation
55 output_noise_power = int.cumtrapz(np.square(o_vnoise[freq_range]), freq
56             ↪ [freq_range])[-1]
57 print('Noise power in frequency range {} - {}: {:.3e} V^2'.format(
58             ↪ cutoffs[0], cutoffs[1], output_noise_power))

```

A.3 Other plots

A.3.1 Tire harmonics

```

1 from math import *
2 import numpy as np
3 import matplotlib.pyplot as plt
4
5 # tire parameters
6

```

```

7  n_grooves = 96
8  r_tire = 0.275 # m
9  c_tire = 2*pi*r_tire # circumference tire (m)
10
11 # phase shift of the grooves on right and left side of the tire
12
13 lr_phase_shift = 4/26*2*pi # rad
14
15 # define axes
16
17 t = np.linspace(0, 0.1, 1000) # seconds
18 speed = np.linspace(0, 40, 500) # m/s
19
20 # plots
21
22 fig = plt.figure(figsize=(10,7))
23 n_harmonics = range(1,6)
24
25 for harmonic in n_harmonics:
26     rot_tire = speed/c_tire # tire rotations/s
27     f_grooves = n_grooves*rot_tire # freq of grooves passing
28     #f_groove_noise = np.sin(2*pi*(f_grooves)*t)+np.sin(2*pi*(
29     ↪ f_grooves)*t+lr_phase_shift) # total freq of grooves
30     plt.plot(speed, harmonic*f_grooves, label='Nth harmonic: {}'.
31     ↪ format(harmonic))
32
33 plt.title('Tire groove noise for harmonics {} - {}'.format(min(
34     ↪ n_harmonics), max(n_harmonics)))
35 plt.legend()
36 plt.grid(True)
37 plt.xlabel('Speed (m/s)')
38 plt.ylabel('Frequency (Hz)')
39 fig.savefig('/home/koen/Documents/Simulation_results/Tire_harmonics/
40     ↪ tire_harmonics_plot.eps', dpi=600, format='eps')
41 plt.show()

```

A.3.2 Permittivity

```

1  import matplotlib.pyplot as plt
2  import numpy as np
3
4  test_freqs = np.array([10e3, 20e3, 30e3, 40e3, 50e3, 60e3, 80e3, 100e3
5  ↪ , 120e3, 140e3, 200e3, 250e3, 300e3, 400e3, 500e3])
6
7  # CAPACITOR WITH RUBBER: FREQUENCY DEPENDENT
8  Vin_new = np.array
9  ↪ ([1.3,1.3,1.3,1.3,1.3,1.3,1.3,1.3,1.3,1.3,1.3,1.3,1.3,1.3,1.3])
10 Vout_new =np.array
11 ↪ ([16.4,20,20.4,20.8,20.6,20.4,20,19.4,18.6,18.2,16.2,14.6,13.2,10.8,9.2])
12 ↪
13
14 Vin_worn = np.array([1.1]*15)

```

```
11 Vout_worn = [12.8, 16.0, 16.8, 17.2, 17.0, 16.8, 16.4, 16.2, 15.6,
    ↪ 15.0, 13.6, 12.2, 11, 9.2, 7.8]
12
13 Vin_air = np.array([2.2]*15)
14 Vout_air = [12.4, 15.8, 16.6, 17, 17, 17, 17, 17, 17, 16.8, 15.8,
    ↪ 14.8, 14.0, 12.7, 10.8]
15
16 figure = plt.figure(figsize=(10,7))
17
18 # New tire plot
19 plt.semilogx(test_freqs ,np.divide(Vout_new , Vin_new))
20
21
22 # Worn tire plot
23 plt.semilogx(test_freqs ,np.divide(Vout_worn , Vin_worn))
24
25
26 # Air plot
27 plt.semilogx(test_freqs ,np.divide(Vout_air , Vin_air))
28
29 plt.xlabel('Frequency (Hz)')
30 plt.ylabel('Ratio Vout/Vin')
31 plt.title('Frequency dependence of new tire , worn tire and air between
    ↪ plates')
32
33 # plt.semilogx(test_freqs [:14], np.diff(np.divide(Vout_new , Vin_new)))
34 # plt.semilogx(test_freqs [:14], np.diff(np.divide(Vout_worn , Vin_worn)
    ↪ ))
35 # plt.semilogx(test_freqs [:14], np.diff(np.divide(Vout_air , Vin_air)))
36
37 plt.legend(['New tire ', 'Worn tire ', 'Air'])
38 plt.grid(True)
39 plt.savefig('/home/koen/Documents/Simulation_results/Ac_sweep/
    ↪ final_permittivity_frequency.eps',dpi=600, format='eps')
40 plt.show()
41
42
43 print(Vout_air)
44 print(Vout_new)
45 print(Vout_worn)
```

Appendix B

Netlists

B.1 LF356

```
* ////////////////////////////////////////////////////////////////////
* (C) National Semiconductor, Inc.
* Models developed and under copyright by:
* National Semiconductor, Inc.

* ////////////////////////////////////////////////////////////////////
* Legal Notice: This material is intended for free software support.
* The file may be copied, and distributed; however, reselling the
* material is illegal

* ////////////////////////////////////////////////////////////////////
* For ordering or technical information on these models, contact:
* National Semiconductor's Customer Response Center
*           7:00 A.M.--7:00 P.M. U.S. Central Time
*           (800) 272-9959
* For Applications support, contact the Internet address:
*   amps-apps@galaxy.nsc.com
* ////////////////////////////////////////////////////////////////////
* User Notes:
*
* 1. Input resistance (Rin) for these JFET op amps is 1TOhm. Rin is
*    modeled by assuming the option GMIN=1TOhm. If a different (non-
*    default) GMIN value is needed, users may recalculate as follows:
*    Rin=(R1||GMIN+R2||GMIN), where R1=R2,
*    to maintain a consistent Rin model.

* ////////////////////////////////////////////////////////////////////
*LF356 Monolithic JFET-Input OP-AMP MACRO-MODEL
* ////////////////////////////////////////////////////////////////////
*
* connections:      non-inverting input
*                   |      inverting input
*                   |      |      positive power supply
*                   |      |      negative power supply
*                   |      |      |      output
```

```

*
*
*
.SUBCKT LF356/NS 1 2 99 50 28
*
*Features:
*Low input bias current = 30pA
*Low input offset current = 3pA
*High input impedance = 1Tohm
*Low input offset voltage = 1mV
*
*****INPUT STAGE*****
*
IOS 2 1 3P
*^Input offset current
R1 1 3 1E12
R2 3 2 1E12
I1 99 4 100U
J1 5 2 4 JX
J2 6 7 4 JX
R3 5 50 20K
R4 6 50 20K
*Fp2=20 MHz
C4 5 6 1.9894E-13
*
*****COMMON MODE EFFECT*****
*
I2 99 50 4.65MA
*^Quiescent supply current
EOS 7 1 POLY(1) 16 49 3E-3 1
*Input offset voltage.^
R8 99 49 50K
R9 49 50 50K
*
*****OUTPUT VOLTAGE LIMITING*****
V2 99 8 2.63
D1 9 8 DX
D2 10 9 DX
V3 10 50 2.63
*
*****SECOND STAGE*****
*
EH 99 98 99 49 1
F1 9 98 POLY(1) VA3 0 0 0 1.5944E7
G1 98 9 5 6 2E-3
R5 98 9 100MEG
VA3 9 11 0
*Fp1=31.96 HZ
C3 98 11 49.9798P
*
*****COMMON-MODE ZERO STAGE*****
*
G4 98 16 3 49 1E-8
L2 98 17 530.52M
R13 17 16 1K

```

```

*
*****OUTPUT STAGE*****
*
F6 99 50 VA7 1
F5 99 23 VA8 1
D5 21 23 DX
VA7 99 21 0
D6 23 99 DX
E1 99 26 99 9 1
VA8 26 27 0
R16 27 28 20
V5 28 25 -.25V
D4 25 9 DX
V4 24 28 -.25V
D3 9 24 DX
*
*****MODELS USED*****
*
.MODEL DX D(IS=1E-15)
.MODEL JX PJF(BETA=1.25E-5 VTO=-2.00 IS=30E-12)
*
.ENDS
*$

```

B.2 AD745

```

* AD745 SPICE Macro-model
* Description: Amplifier
* Generic Desc: 9.6/30V, JFET, OP, Low Noise, Fast, 1X
* Developed by: ARG / ADSC
* Revision History: 08/10/2012 - Updated to new header style
* 2.0 (10/1995) - Changed the negative zero circuit to correspond to the new design
* which eliminates the negative capacitor value.
* Copyright 1992, 2012 by Analog Devices.
*
* Refer to http://www.analog.com/Analog\_Root/static/techSupport/designTools/spiceMod
* indicates your acceptance with the terms and provisions in the License Statement.
*
* BEGIN Notes:
*
* Not Modeled:
*
* Parameters modeled include:
*
* END Notes
*
* Node assignments
*
*           non-inverting input
*           |   inverting input
*           |   |   positive supply
*           |   |   |   negative supply
*           |   |   |   |   output
*           |   |   |   |

```

```

.SUBCKT AD745      3  2  99  50  37
*
* INPUT STAGE AND POLE AT 54MHZ
*
I1  97  1  1
J1  5  2  1  JX
J2  6  4  1  JX
CIN 2  3  20E-12
IOS  3  2  15E-12
EN  7  3  9  0  1
GN1 0  2  12  0  1E-6
GN2 0  3  15  0  1E-6
EOS  4  7  POLY(1) 31  52  100E-6  1
R1  5  51  86.842E-3
R2  6  51  86.842E-3
C1  5  6  16.969E-9
EPOS 97  0  99  0  1
ENEG 51  0  50  0  1
EREF 98  0  52  0  1
*
* VOLTAGE NOISE SOURCE WITH FLICKER NOISE
*
VN1  8  0  DC 2
VN2  0  10 DC 2
DN1  8  9  DEN
DN2  9  10 DEN
*
* CURRENT NOISE SOURCE WITH FLICKER NOISE
*
VN3  11  0  DC 10
VN4  0  13  DC 10
DN3  11  12  DIN
DN4  12  13  DIN
*
* CURRENT NOISE SOURCE WITH FLICKER NOISE
*
VN5  14  0  DC 10
VN6  0  16  DC 10
DN5  14  15  DIN
DN6  15  16  DIN
*
* GAIN STAGE AND DOMINANT POLE AT 5.727HZ
*
R3  17  98  347.368E3
C2  17  98  80E-9
G1  98  17  5  6  11.515
V1  97  18  .027
V2  19  51  1.193
D1  17  18  DX
D2  19  17  DX
*
* POLE AT 30MHZ
*
R4  23  98  1

```

```

C3  23  98  5.305E-9
G2  98  23  17 52 1
*
* POLE AT 30MHZ
*
R5  24  98  1
C4  24  98  5.305E-9
G3  98  24  23 52 1
*
* NEGATIVE ZERO AT -54MHZ
*
R6  25  26  1
R7  26  98  1E-6
E1  25  98  24 52 1E6
VX1 84  0  DC 0
EX1 83  0  25 26 1
FX1 25  26  VX1 -1
CX1 83  84  2.947E-9
*
* POLE / ZERO AT 2MHZ / 2.25MHZ
*
R8  27  98  1
R9  27  28  8
C6  28  98  8.842E-9
G4  98  27  26 52 1
*
* COMMON MODE GAIN STAGE WITH ZERO AT 10KHZ
*
E2  29  30  2 52 0.5
E3  30  98  3 52 0.5
R10 29  31  1
R11 31  98  7.943E-6
C7  29  31  15.916E-6
*
* REFERENCE NODE AND OUTPUT STAGE
*
RMP1 97  52  1
RMP2 52  51  1
GSY 99  50  POLY(1) 99 50 7.625E-3 12.5E-6
R13 99  36  200
R14 36  50  200
L1  36  37  1E-10
G5  34  50  27 36 5E-3
G6  35  50  36 27 5E-3
G7  36  99  99 27 5E-3
G8  50  36  27 50 5E-3
V3  32  36  2.922
V4  36  33  1.460
D3  27  32  DX
D4  33  27  DX
D5  99  34  DX
D6  99  35  DX
D7  50  34  DY
D8  50  35  DY

```

```

F1 36 0 V3 1
F2 0 36 V4 1
*
* MODELS USED
*
.MODEL JX PJF(BETA=66.299, VTO=-1.5 IS=150E-12)
.MODEL DX D(IS=1E-15)
.MODEL DY D(IS=1E-15, BV=50)
.MODEL DEN D(RS=1.015E3, KF=4.311E-15, AF=1)
.MODEL DIN D(RS=5.277E3, KF=42.593E-15, AF=1)
.ENDS AD745

```

B.3 Charge amplifier with compensation

```

* /home/koen/Documents/Elektro/KiCad/c_amp_2/c_amp_2.cir

* Sheet Name: /
XLF_356 Net_Cc1-Pad1_ Net_Cf1-Pad1_ VCC.n VDD.n vout LF356/NS
Cf1 Net_Cf1-Pad1_ Vout 1p
Cc1 Net_Cc1-Pad1_ GND 1p
Ct1 Net_Cf1-Pad1_ Net_Ct1-Pad2_ 3.5p
Rc1 Net_Cc1-Pad1_ GND 10Meg
Rf1 Net_Cf1-Pad1_ Vout 10Meg
Rt1 vin Net_Ct1-Pad2_ 10

* Sources
VCC VCC.n 0 DC 15
VDD VDD.n 0 DC -15
VIN vin 0 dc 0 ac 1

* Simulation parameters
.options noacct temp=21 tnom=21 nomod nopage
.ac dec 50 1k 10Meg $ ac analysis from 1-10 MHz, 50 data points per decade
.print ac v(vout)

* netlist containing .subckt of LF356
.include lf356.cir

.end

```

B.4 Charge amplifier without compensation

```

* /home/koen/Documents/Elektro/KiCad/c_amp_2/c_amp_2_no_comp.cir

* Sheet Name: /
XLF_356 GND Net_Cf1-Pad1_ VCC.n VDD.n vout LF356/NS
Cf1 Net_Cf1-Pad1_ Vout 1p
Ct1 Net_Cf1-Pad1_ Net_Ct1-Pad2_ 3.5p
Rf1 Net_Cf1-Pad1_ Vout 10Meg
Rt1 vin Net_Ct1-Pad2_ 10

* Sources

```

```
VCC VCC.n 0 DC 15
VDD VDD.n 0 DC -15
VIN vin 0 dc 0 ac 1
```

```
* Simulation parameters
```

```
.options noacct temp=21 tnom=21 nomod nopage
```

```
.ac dec 50 1k 10Meg $ ac analysis from 1-10 MHz, 50 data points per decade
```

```
.print ac v(vout)
```

```
* netlist containing .subckt of LF356
```

```
.include lf356.cir
```

```
.end
```

Appendix C

Shell script

```
#!/bin/sh
# Author: Koen Goedemondt
# File parser for ngspice noise analysis output files

export NGSPICE_INPUT_DIR='/home/koen/Documents/Elektro/Netlists'
export SPICE_ASCII_RAWFILE='1'
infile=$1
outfile=$2
working_dir='/home/koen/Documents/Elektro/Netlists'
if [ $# -eq 3 ]
then
    working_dir=$3
fi
ngspice -b $infile -r ${working_dir}/${outfile}
sed -n '/^Values: /,/^Values: /p' ${working_dir}/${outfile} |
grep -Po '\d+\.\d+e[-+]?[d]{2}' | xargs -n 3 > "${outfile%.*}.txt"
```

Bibliography

- [1] M. Alderliesten, M. Brakel, S. Groot, F. Immerzeel, and T. Verboon, "Het monitoren van bandenconditie," 2009.
- [2] Murata Power Solutions, *50 mV and 100 mV base-mounted DC shunts Datasheet*.
- [3] IMC Meßsysteme GmbH, *μ -CANSAS-V1/V4 technical specification*, 9 2009. Version 1.3.
- [4] Honeywell, *MICRO SWITCH Sensing and Control: Hall Effect Sensing and Application*.
- [5] E. Ramsden, *Hall-effect sensors: theory and application*. Elsevier, 01 2006.
- [6] J. E. Lenz, "A review of magnetic sensors," vol. 78, pp. 973 – 989, 07 1990.
- [7] "The basics of current sensors." <https://www.digikey.com/en/articles/techzone/2012/sep/the-basics-of-current-sensors>. Accessed: 18-6-2018.
- [8] W. Thomson, "On the electro-dynamic qualities of metals: Effects of magnetization on the electric conductivity of nickel and of iron," January 1856.
- [9] T. McGuire and R. Potter, "Anisotropic magnetoresistance in ferromagnetic 3d alloys," *IEEE Transactions on Magnetics*, July 1975.
- [10] D. Mapps, "Magnetoresistive sensors," *Sensors and Actuators A: Physical*, vol. 59, no. 1, pp. 9 – 19, 1997. 1st European magnetic sensors and actuators conference.
- [11] T. Shek and J. Vliegthart, "Nuna sensor system," 2018.
- [12] O. Singh and S. K. Gupta, "A review on recent mppt techniques for photovoltaic system," in *2018 IEEMA Engineer Infinite Conference (eTechNxT)*, pp. 1–6, March 2018.
- [13] Sensitec, *CMS3000 Magnetoresistive Current Sensor product family datasheet*, May 2017.
- [14] "Farnell hall effect current sensor overview." <http://nl.farnell.com/c/sensors-transducers/sensors/current-sensors>. Accessed: 2018-06-17.
- [15] LEM, *LTSR 15-NP Current transducer datasheet 110214/13*.
- [16] Maxim Integrated, *MAX4238/4239 Ultra-Low Offset/Drift, Low-Noise, Precision SOT23 Amplifiers*, February 2018.
- [17] "Bridgestone World Solar Challenge 2019 regulations," June 2018.
- [18] G. W. Parker, "Electric field outside a parallel plate capacitor," 2002.
- [19] B. Babu, D. E. Selvaraj, R. Srinivas, B. G. Prakash, R. V. Prakash, E. Muthupandi, and R. Balakumar, "Analysis of relative permittivity and tan delta characteristics of silicone rubber based nanocomposites," 2012.
- [20] S.-J. H. Yeong-Jyh Lin, "Temperature prediction of rolling tires by computer simulation," 2004.
- [21] L. H. Ford, "The effect of humidity on the calibration of precision air capacitors," 1948.

- [22] Texas Instruments, *LFx5x JFET Input Operational Amplifiers Datasheet*, 5 2000. Revised November 2015.
- [23] Analog devices, *Ultralow Noise, High Speed, BiFET Op Amp, AD745*, 2002.
- [24] Linear technology, *LT1026 Voltage Converter*.
- [25] H. Vogt, M. Hendrix, and P. Nenzi, *Ngspice Users Manual*. Sourceforge, May 2018.